Helmholtz-Zentrum Geesthacht
Zentrum für Material- und Küstenforschung

Preprint 2011

An incremental minimization principle suitable for the analysis of low cycle fatigue in metals: a coupled ductile-brittle damage model

O. Kintzel and J. Mosler

This is a preprint of an article accepted by:

Computer Methods in Applied Mechanics and Engineering

(2011)

Helmholtz-Zentrum Geesthacht
Materials Mechanics

An incremental minimization principle suitable for the analysis of low cycle fatigue in metals: a coupled ductile-brittle damage model

O. Kintzel and J. Mosler

Materials Mechanics
Institute of Materials Research
Helmholtz-Zentrum Geesthacht
D-21502 Geesthacht, Germany
E-Mail: joern.mosler@hzg.de

SUMMARY

The present paper is concerned with a novel *variational constitutive update* suitable for the analysis of low cycle fatigue in metals. The underlying constitutive model originally advocated in (1) accounts for plastic deformation as well as for damage accumulation. The latter is captured by a combination of two constitutive models. While the first of those is associated with ductile damage, the second material law is related to a quasi-brittle response. The complex overall model falls into the range of so-called *generalized standard materials* and thus, it is thermodynamically consistent. However, since the evolution equations are non-associative, it does not show an obvious variational structure. By enforcing the flow rule as well as the evolution equations through a suitable parameterization, a minimization principle can be derived nevertheless. Discretized in time, this principle is employed for developing an effective numerical implementation. Since the mechanical subproblems corresponding to ductile damage and that of quasi-brittle damage are uncoupled, an efficient staggered scheme can be elaborated. Within both steps, Newton's method is applied. While the evolution of the quasi-brittle damage requires only the computation of a one-dimensional optimization problem, the ductile damage model is defined by a numerically more expensive tensor-valued variable. For further increasing the numerical performance of the respective minimization principle, a closed-form solution for the inverse of the Hessian matrix is derived. By numerically analyzing the prediction of mesocrack initiation in low-cycle fatigue simulations, the performance of the resulting algorithm is demonstrated.

1 INTRODUCTION

Fatigue failure can have a strong influence on the design of engineering structures and the corresponding safety measures during their service life. This holds in particular for structures subjected to alternate loading with high amplitudes as found, e.g., in transportation vehicles like airplanes or cars during critical situations. Furthermore, especially in those structures, the demand for innovative lightweight and high-strength materials with superior mechanical properties is high. For this reason, high-strength aluminum alloys are widely used in the aerospace industry, e.g., for wing reinforcement or in aircrafts' fuselages, since they combine a good fatigue performance with high strength.

A frequently applied high-strength aluminum alloy is Al2024-T351. A comprehensive discussion of the relevant damage mechanisms of this material can be found in (1).

According to the microstructural assessments reported in the cited paper, the material behavior of Al2024-T351 shows an interplay between ductile and quasi-brittle damage – particularly, in case of fatigue processes at high stress levels. Here, ductile damage is understood as damage caused by micro-void evolution and coalescence, while brittle damage is defined as caused by small fatigue crack growth. For the modeling of such a mechanical response which is also typical for other high-strength alloys, a novel ductile-brittle damage model was recently proposed in (1; 2). The foundation of this model is a phenomenologically-based continuum damage mechanics (CDM) framework in which damage is continuously distributed within representative volume cells. The ductile damage part is modeled similarly to a proposition of Lemaitre (3) governed mainly by the evolution of the plastic strains, while quasi-brittle damage is driven by the energy release and can be activated without plastic deformation. Without going too much into detail, the quasi-brittle part shares some analogies to the well-known Paris law (4). Such analogies allow an effective material parameter determination. The excellent predictive capabilities of the resulting constitutive model are reported in (1; 2).

Clearly, the application of constitutive models such as that described before to the analysis of engineering structures requires an efficient numerical implementation. Frequently, the by now classical *return-mapping scheme* is employed for that purpose, cf. (5). Within this first-order accurate scheme, the evolution equations as well as the flow rule are enforced. Other physically relevant principles are ignored. By way of contrast, an alternative, variationally consistent method was proposed by Ortiz and co-workers, see (6; 7). This approach is based on minimizing the stress power. As shown in (8; 9), this variational principle is equivalent to the postulate of maximum dissipation in case of rate-independent materials. Due to the underlying variational basis, such models are referred to as *variational constitutive updates*, cf. (10–13).

In general, variational principles enjoy a long tradition in mechanics. As one of the first, a variational principle suitable for the modeling of crack extension in brittle materials was proposed by Griffith (14). Within that principle, a pre-existing crack is assumed to propagate with infinitesimal length provided the elastic energy released is greater than that spent for new crack surfaces. In order to bypass the well-known defects of Griffith's original idea such as the requirement of a pre-existing crack, a modified energy-based criterion based on a finite crack extension was proposed in (15–17). A comprehensive overview of such models can be found in (18). For a mathematically rigorous analysis, the interested reader is referred to (19; 20).

Within Griffith's original model as well as within the respective extensions, a brittle solid is presumed. Instead, cohesive zone models are frequently applied for quasi-brittle materials showing a continuous softening response. Here and in contrast to (14), the interface energy characterizing the mechanical response is not constant any more. Variationally consistent cohesive zone models in line with the pioneering work (14) are discussed in (21–23). A continuous approximation of the discrete cracks by using a gradient-type formulation can be found in (24).

According to the literature review presented in the previous paragraphs, variational principles suitable for the modeling of material degradation are not new in general. However, the cited models are suitable for monotonic loading only and do not apply to cyclic loading or low cycle fatigue in particular. In the present paper, a novel variationally consistent model inspired by the pioneering work of Griffith (14) which is suitable for the analysis of low cycle fatigue is developed.

In addition to the physically and mathematically elegant structure of the aforementioned variational principles, such methods show further important advantages compared

to conventional material descriptions, cf. (9). In the context of the low cycle fatigue model advocated in (1), at least three of such advantages have to be mentioned explicitly. The first of those is the numerical efficiency. More precisely, it will be shown that the resulting variational constitutive update is significantly faster than a classical return-mapping scheme. Since both methods rely on Newton's scheme, the efficiency must be ascribed to the mathematically and physically well-posed structure of the variationally consistent numerical implementation. The second advantage is concerned with the interplay between ductile and brittle damage mechanisms. Within the present model, the decomposition of material damage into the different aforementioned parts is assumed as constant, i.e., 86% of the total damage are due to micro-void evolution and coalescence, while 14% are related to small fatigue crack growth. Evidently, such an assumption is only a relatively simple approximation and not very realistic. However, in case of variational constitutive updates, energy minimization is the overriding physical principle and thus, it is natural to choose that ratio between the different damage contributions which is energetically most favorable. Although such an extended model will not be discussed in the present paper, some additional remarks will be given. The final advantage of a variational formulation to be noted here is the naturally induced micro-to-macro transition (25). More specifically, the principle of energy equivalence can be used to relate the purely phenomenological model (1) to a physically more sound micromechanical description, see (25).

A careful analysis of the model presented in (1) reveals that its reformulation into a variationally consistent framework is not straightforward. The probably most serious problems are related to the non-associative evolution equations and the complexity of the model. Concerning the first point, no obvious variational structure exists for models not obeying the normality rule. For that purpose, an extended principle of maximum dissipation was very recently introduced in (9; 26) in which the non-associative flow rule as well as the evolution equations were enforced by a suitable parameterization, cf. (13). An adapted version of this approach will also be applied in the present paper. The second problem associated with the model proposed in (1) is its complexity. So far, variational constitutive updates have only been derived for relatively simple constitute models, cf. (6; 7; 9–13). A complex coupled elastoplastic damage model has not been considered yet. For reducing this complexity, a two-step staggered scheme has been elaborated. Within the first step, the purely ductile damage model is considered, whereas quasi-brittle damage accumulation may be active during the second step. Both subproblems are solved by a numerically efficient Newton iteration. While the evolution of the quasi-brittle damage requires only the computation of a one-dimensional optimization problem, the ductile damage model is defined by a numerically more expensive tensor-valued variable. Clearly, a boost in performance could be obtained by deriving a closed-form solution for the inverse of the Hessian matrix. Unfortunately, this matrix is singular. One reason for this singularity is the constraint imposed by the deviatoric flow rule. By defining a physically sound pseudoinverse, a closed-form solution of the respective Hessian matrix can be derived nevertheless. This results eventually in very efficient numerical formulation – even in comparison to the classical return-mapping scheme.

The paper is structured as follows: In Section 2, the ductile-brittle damage model originally proposed in (1) is described. The variational reformulation of this model is discussed in Section 3. Based on this reformulation, a novel effective numerical implementation is elaborated in Section 4. Finally, the performance of the resulting algorithmic formulation is critically analyzed in Section 5.

2 A novel ductile-brittle damage formulation in a nutshell

In the present section, the novel ductile-brittle damage formulation proposed in (1) is outlined. First, the ductile and brittle damage models are treated separately. Subsequently, they are coupled. Throughout the paper, a geometrically linear setting is used in which the strains $\boldsymbol{\epsilon}$ are decomposed into an elastic part $\boldsymbol{\epsilon}^{\mathrm{e}}$ and a plastic part $\boldsymbol{\epsilon}^{\mathrm{p}}$, i.e., $\boldsymbol{\epsilon} = \boldsymbol{\epsilon}^{\mathrm{e}} + \boldsymbol{\epsilon}^{\mathrm{p}}$.

2.1 The ductile damage model

For capturing ductile damage degradation, a model similar to one originally proposed by Lemaitre is used, cf. (3). Conceptually, it is assumed that the damage evolution depends directly on the plastic strain rates. The resulting model falls into the range of so-called *generalized standard materials* (see (27)) and thus, it is thermodynamically consistent.

For guaranteeing thermodynamical consistency, the model is based on a Helmholtz energy functional Ψ. Analogously to (3), Ψ is chosen as

$$\Psi(\boldsymbol{\epsilon}^{\mathrm{e}}, \boldsymbol{\alpha}_{\mathrm{k}}, \alpha_{\mathrm{i}}, D) = (1-D)\left(\frac{\boldsymbol{\epsilon}^{\mathrm{e}} : \mathbb{C} : \boldsymbol{\epsilon}^{\mathrm{e}}}{2} + H_{\mathrm{k}}\,\frac{\boldsymbol{\alpha}_{\mathrm{k}} : \boldsymbol{\alpha}_{\mathrm{k}}}{2} + H_{\mathrm{i}}\,\frac{\alpha_{\mathrm{i}}^2}{2}\right) . \tag{1}$$

Here and henceforth, the subscripts $(\bullet)_{\mathrm{k}}$ and $(\bullet)_{\mathrm{i}}$ denote quantities corresponding to kinematic and isotropic hardening, respectively. $\boldsymbol{\alpha}_{\mathrm{k}}$ and α_{i} are strain-like internal variables associated with hardening and H_{k} and H_{i} are the related hardening moduli, $D \in [0,1]$ is a scalar-valued and evolving damage variable and $\mathbb{C} = \kappa\,\mathbf{1}\otimes\mathbf{1} + 2\,\mu\,\mathbb{P}_{\mathrm{dev}}$ is the elastic stiffness tensor depending on the bulk modulus κ and the shear modulus μ as well as on the deviatoric projection tensor $\mathbb{P}_{\mathrm{dev}}$. In generalization to the framework in (3), the damage variable D in Eq. (1) does not only affect the elastic strain energy part, but also that related to hardening, see Remark 1. Based on Eq. (1), the dual or energetically conjugate variables $(\boldsymbol{\sigma}^{\mathrm{e}}, \boldsymbol{Q}_{\mathrm{k}}, Q_{\mathrm{i}}, Y)$ to $(\boldsymbol{\epsilon}^{\mathrm{e}}, \boldsymbol{\alpha}_{\mathrm{k}}, \alpha_{\mathrm{i}}, D)$ can be defined in standard manner. More specifically,

$$Y = -\partial_D \Psi = \left(\frac{\boldsymbol{\epsilon}^{\mathrm{e}} : \mathbb{C} : \boldsymbol{\epsilon}^{\mathrm{e}}}{2} + H_{\mathrm{k}}\,\frac{\boldsymbol{\alpha}_{\mathrm{k}} : \boldsymbol{\alpha}_{\mathrm{k}}}{2} + H_{\mathrm{i}}\,\frac{\alpha_{\mathrm{i}}^2}{2}\right) \tag{2}$$

and

$$\begin{aligned} \boldsymbol{\sigma} &= \partial_{\boldsymbol{\epsilon}^{\mathrm{e}}}\Psi = (1-D)\mathbb{C} : \boldsymbol{\epsilon}^{\mathrm{e}} = -\partial_{\boldsymbol{\epsilon}^{\mathrm{p}}}\Psi \\ \mathbf{Q}_{\mathrm{k}} &= -\partial_{\boldsymbol{\alpha}_{\mathrm{k}}}\Psi = -(1-D)H_{\mathrm{k}}\,\boldsymbol{\alpha}_{\mathrm{k}} \\ Q_{\mathrm{i}} &= -\partial_{\alpha_{\mathrm{i}}}\Psi = -(1-D)H_{\mathrm{i}}\,\alpha_{\mathrm{i}}. \end{aligned} \tag{3}$$

In Eqs. (2) and (3), Y is the energy release, $\boldsymbol{\sigma}$ is the stress tensor and $\mathbf{Q}_{\mathrm{k}}$ and Q_{i} are stress-like internal variables conjugate to $\boldsymbol{\alpha}_{\mathrm{k}}$ and α_{i}. According to Eq. (2) and different to the assumption in (3), where only the elastic strain energy part was released, all elastoplastic strain energy parts are taken into account for the driving force of damage accumulation.

A further common assumption, related to the effective stress concept, is that ductile damage has no appreciable effect on plastic slip, i.e., plastic slip is not disturbed by damage profoundly. Making this assumption, the yield function ϕ^{p} defining the space of admissible stresses must not depend on the damage variable D. As a result and by introducing the effective stress-like variables $(\tilde{\boldsymbol{\sigma}},\ \tilde{\mathbf{Q}}_{\mathrm{k}},\ \tilde{Q}_{\mathrm{i}})$ as counterparts to $(\boldsymbol{\sigma},\ \mathbf{Q}_{\mathrm{k}},\ Q_{\mathrm{i}})$ via

$$\tilde{\boldsymbol{\sigma}} = \frac{\boldsymbol{\sigma}}{(1-D)}\ , \quad \tilde{\mathbf{Q}}_{\mathrm{k}} = \frac{\mathbf{Q}_{\mathrm{k}}}{(1-D)}\ , \quad \tilde{Q}_{\mathrm{i}} = \frac{Q_{\mathrm{i}}}{(1-D)} \tag{4}$$

$\phi^{\mathrm{p}} = \phi^{\mathrm{p}}(\tilde{\boldsymbol{\sigma}}, \tilde{\mathbf{Q}}_{\mathrm{k}}, \tilde{Q}_{\mathrm{i}})$ holds. As a prototype model, the von Mises-type yield function

$$\phi^{\mathrm{p}} = \sqrt{\frac{3}{2}\,\mathrm{dev}(\tilde{\boldsymbol{\sigma}} - \tilde{\mathbf{Q}}_{\mathrm{k}}) : \mathrm{dev}(\tilde{\boldsymbol{\sigma}} - \tilde{\mathbf{Q}}_{\mathrm{k}})} - (\tilde{Q}_{\mathrm{i}} + Q_0^{\mathrm{eq}}) \leq 0, \tag{5}$$

with $\mathrm{dev}(\bullet) := \mathbb{P}_{\mathrm{dev}} : (\bullet)$ is considered in what follows. Here, Q_0^{eq} is the initial yield limit. It bears emphasis that the framework proposed in (1) can also be applied to other yield functions, i.e., Eq. (5) is not mandatory.

As pointed out, e.g., in (3), the effective stress measures (4) can be consistently derived from a fictitious un-damaged material state. For that purpose, the principle of strain equivalence stating $\tilde{\boldsymbol{\epsilon}}^{\mathrm{e}} = \boldsymbol{\epsilon}^{\mathrm{e}}$, $\tilde{\boldsymbol{\epsilon}}^{\mathrm{p}} = \boldsymbol{\epsilon}^{\mathrm{p}}$, $\tilde{\boldsymbol{\alpha}}_{\mathrm{k}} = \boldsymbol{\alpha}_{\mathrm{k}}$ and $\tilde{\alpha}_{\mathrm{i}} = \alpha_{\mathrm{i}}$ is used. With this principle, the Helmholtz energy of that un-damaged material state is given by

$$\tilde{\Psi}(\tilde{\boldsymbol{\epsilon}}^{\mathrm{e}}, \tilde{\boldsymbol{\alpha}}_{\mathrm{k}}, \tilde{\alpha}_{\mathrm{i}}) = \frac{\tilde{\boldsymbol{\epsilon}}^{\mathrm{e}} : \mathbb{C} : \tilde{\boldsymbol{\epsilon}}^{\mathrm{e}}}{2} + H_{\mathrm{k}}\,\frac{\tilde{\boldsymbol{\alpha}}_{\mathrm{k}} : \tilde{\boldsymbol{\alpha}}_{\mathrm{k}}}{2} + H_{\mathrm{i}}\,\frac{\tilde{\alpha}_{\mathrm{i}}^2}{2} \tag{6}$$

and thus, the stress-like variables ($\tilde{\boldsymbol{\sigma}}^{\mathrm{e}}$, $\tilde{\boldsymbol{Q}}_{\mathrm{k}}$ $\tilde{Q}_{\mathrm{i}}$) conjugate to (($\tilde{\boldsymbol{\epsilon}}^{\mathrm{e}}$, $\tilde{\boldsymbol{\epsilon}}^{\mathrm{p}}$), $\tilde{\boldsymbol{\alpha}}_{\mathrm{k}}$ $\tilde{\alpha}_{\mathrm{i}}$) result in

$$\begin{aligned} \tilde{\boldsymbol{\sigma}} &= \partial_{\tilde{\boldsymbol{\epsilon}}^{\mathrm{e}}}\tilde{\Psi} = \mathbb{C} : \boldsymbol{\epsilon}^{\mathrm{e}} = -\partial_{\tilde{\boldsymbol{\epsilon}}^{\mathrm{p}}}\tilde{\Psi} \\ \tilde{\mathbf{Q}}_{\mathrm{k}} &= -\partial_{\tilde{\boldsymbol{\alpha}}_{\mathrm{k}}}\tilde{\Psi} = -H_{\mathrm{k}}\,\boldsymbol{\alpha}_{\mathrm{k}} \\ \tilde{Q}_{\mathrm{i}} &= -\partial_{\tilde{\alpha}_{\mathrm{i}}}\tilde{\Psi} = -H_{\mathrm{i}}\,\tilde{\alpha}_{\mathrm{i}} \end{aligned} \tag{7}$$

being equivalent to Eqs. (4).

For completing the constitutive model, suitable evolution equations for the internal variables are required. Such equations have to fulfill the second law of thermodynamics. Considering isothermal, purely mechanical processes, this law can be written as

$$\mathcal{D} = \boldsymbol{\sigma} : \dot{\boldsymbol{\epsilon}} - \dot{\Psi} = \boldsymbol{\sigma} : \dot{\boldsymbol{\epsilon}}^{\mathrm{p}} + \mathbf{Q}_{\mathrm{k}} : \dot{\boldsymbol{\alpha}}_{\mathrm{k}} + Q_{\mathrm{i}}\,\dot{\alpha}_{\mathrm{i}} + Y\,\dot{D} \geq 0\ . \tag{8}$$

Here, a superposed dot represents the material time derivative. An elegant and effective method for guaranteeing Ineq. (8) is provided by the framework of *generalized standard materials*, cf. (27). According to that framework, Ineq. (8) is automatically fulfilled, if the evolution equations are gradients of a convex potential denoted as $\bar{\phi}^{\mathrm{p}}$ in what follows. In line with (1), the choice

$$\bar{\phi}^{\mathrm{p}} = \phi^{\mathrm{p}} + \frac{Y^M}{M\,S_1\,(1-D)} + \frac{B_{\mathrm{k}}}{H_{\mathrm{k}}}\,\frac{\tilde{\mathbf{Q}}_{\mathrm{k}} : \tilde{\mathbf{Q}}_{\mathrm{k}}}{2} + \frac{B_{\mathrm{i}}}{H_{\mathrm{i}}}\,\frac{\tilde{Q}_{\mathrm{i}}^2}{2}\ . \tag{9}$$

is made. The first term in Eq. (9) corresponds to the classical associative evolution equations, while the second term defines the evolution of the damage variable. This choice is similar to that previously advocated by Lemaitre, cf.(3). It depends on the material parameters S_1 and M. The remaining and outermost right-hand side terms, involving the stress-like variables $\tilde{\boldsymbol{Q}}_{\mathrm{k}}$ and $\tilde{Q}_{\mathrm{i}}$, define the non-associative parts of the frequently applied Armstrong-Frederick-type hardening model. These terms depend on the material parameters B_{k} and B_{i} which define the saturated values of $\tilde{\boldsymbol{Q}}_{\mathrm{k}}$ and $\tilde{Q}_{\mathrm{i}}$. Combining Eq. (9) with the framework of generalized standard materials, the evolution equations can be computed as

$$\dot{\boldsymbol{\epsilon}}^{\mathrm{p}} = \lambda^{\mathrm{p}}\partial_{\boldsymbol{\sigma}}\bar{\phi}^{\mathrm{p}} = \frac{\lambda^{\mathrm{p}}}{(1-D)}\,\mathbf{n} \tag{10}$$

$$\dot{\boldsymbol{\alpha}}_{\mathrm{k}} = \lambda^{\mathrm{p}}\partial_{\mathbf{Q}_{\mathrm{k}}}\bar{\phi}^{\mathrm{p}} = -\frac{\lambda^{\mathrm{p}}}{(1-D)}\,(\mathbf{n} + B_{\mathrm{k}}\,\boldsymbol{\alpha}_{\mathrm{k}}) \tag{11}$$

$$\dot{\alpha}_{\mathrm{i}} = \lambda^{\mathrm{p}}\partial_{Q_{\mathrm{i}}}\bar{\phi}^{\mathrm{p}} = -\frac{\lambda^{\mathrm{p}}}{(1-D)}\,(1 + B_{\mathrm{i}}\,\alpha_{\mathrm{i}}) \tag{12}$$

$$\dot{D} = \lambda^{\mathrm{p}}\partial_{Y}\bar{\phi}^{\mathrm{p}} = \frac{\lambda^{\mathrm{p}}}{(1-D)}\,\frac{Y^{M-1}}{S_1}\ . \tag{13}$$

In Eq. (10), $\mathbf{n} := \partial\bar{\phi}^{\mathrm{p}}/\partial\tilde{\boldsymbol{\sigma}}$ is the flow direction. Evolution equations (10)–(13) are constrained by the Karush-Kuhn-Tucker conditions

$$\lambda^{\mathrm{p}} \geq 0 \ , \quad \phi^{\mathrm{p}} \leq 0 \ , \quad \lambda^{\mathrm{p}}\,\phi^{\mathrm{p}} = 0 \ , \tag{14}$$

where λ^{p} is the scalar-valued consistency parameter often referred to as the plastic multiplier. Alternatively, Eqs. (10)–(13) can be rewritten as

$$\dot{\boldsymbol{\epsilon}}^{\mathrm{p}} = p\,\mathbf{n}, \quad \dot{\boldsymbol{\alpha}}_{\mathrm{k}} = -p\,(\mathbf{n} + B_{\mathrm{k}}\,\boldsymbol{\alpha}_{\mathrm{k}}), \quad \dot{\alpha}_{\mathrm{i}} = -p\,(1 + B_{\mathrm{i}}\,\alpha_{\mathrm{i}}), \quad \dot{D} = p\,\frac{Y^{M-1}}{S_1} \tag{15}$$

with $p := \sqrt{\frac{2}{3}}\,||\dot{\boldsymbol{\epsilon}}^{\mathrm{p}}||$. The advantage of this parameterization is that it does not depend on the damage variable D – at least, not explicitly. Consequently, the ductile damage model can be conveniently decomposed into two subproblems with reduced complexity, i.e., Eqs. $(15)_1$-$(15)_3$ are considered first. Since they are formally identical to standard plasticity without damage accumulation, they can be solved in standard manner. Subsequently, Eq. $(15)_4$ is computed.

Remark 1 *According to Helmholtz energy (1), the damage variable D in Eq. (1) does not only modify the elastic strain energy part, but also those related to plasticity. Thus, the total energy release (2) contains in addition to the elastic part, also two terms associated with hardening. Assuming the energy stored in the material in form of dislocation structures (e.g. dislocation pile-up energy) may be released during damage processes similarly to the elastic energy, Helmholtz energy (1) is physically sound. Furthermore and as shown in Subsection 3.4, Helmholtz energy (1) leads to a more simple variational formulation than the original model proposed by Lemaitre (3).*

2.2 The brittle damage model

In addition to ductile damage caused by void growth, high strength aluminum alloys can also show quasi-brittle material degradation. For describing this phenomenon, a novel model was recently proposed in (1). It has been inspired by analogies to the constitutive law discussed in the previous subsection. In line with Eq. (1), the Helmholtz energy of that model is defined by

$$\Psi = (1 - D)\,Y + H_{\Gamma}\,\frac{\alpha_{\Gamma}^2}{2} + H_{\mathrm{b}}\,\frac{\alpha_{\mathrm{b}}^2}{2} \ . \tag{16}$$

In Eq. (16), Y is the energy release (see Eq. (2)), α_{Γ} and α_{b} are internal variables associated with hardening/softening due to damage accumulation and H_{Γ} and H_{b} are the respective hardening/softening moduli. Following standard thermodynamical arguments, the dual variables of (α_{Γ}, α_{b}, Y) are introduced by the state equations

$$Y = -\partial_D \Psi \ , \quad \Gamma = -\partial_{\alpha_{\Gamma}} \Psi = -H_{\Gamma}\,\alpha_{\Gamma} \ , \quad Q_{\mathrm{b}} = -\partial_{\alpha_{\mathrm{b}}} \Psi = -H_{\mathrm{b}}\,\alpha_{\mathrm{b}} \ . \tag{17}$$

Although formally identical to the ductile damage model, the internal variables $(Y, \Gamma, Q_{\mathrm{b}})$ are now energy-like. Based on such variables, a yield or rather failure function ϕ^{b} is introduced. Accounting for an isotropic as well as a kinematic transformation of the failure surface $\phi^{\mathrm{b}} = 0$,

$$\phi^{\mathrm{b}} = \frac{|Y^N - \Gamma|}{S_2} - (Q_{\mathrm{b}} + Q_{\mathrm{b0}}) \leq 0 \tag{18}$$

is a suitable choice. Here, N and S_2 are material parameters, while $Q_{\mathrm{b}0}$ defines the energy threshold of the endurance limit.

In case of loading characterized by $\phi^{\mathrm{b}} = 0$ and $\dot{\phi}^{\mathrm{b}} = 0$, the internal variables evolve. For guaranteeing thermodynamically sound evolution equations fulfilling the second law of thermodynamics

$$\mathcal{D} = \Gamma\,\dot{\alpha}_\Gamma + Q_{\mathrm{b}}\,\dot{\alpha}_{\mathrm{b}} + Y\,\dot{D} \geq 0\ , \tag{19}$$

the framework of generalized standard materials (see (27)) is again employed. Thus, the evolution equations are gradients of a convex potential denoted as $\bar{\phi}^{\mathrm{b}}$. Following (1) and Eq. (9), $\bar{\phi}^{\mathrm{b}}$ is additively decomposed into the failure function ϕ^{b} and additional quadratic Armstrong-Frederick-type terms, i.e.,

$$\bar{\phi}^{\mathrm{b}} = \phi^{\mathrm{b}} + \frac{B_\Gamma}{H_\Gamma}\,\frac{\Gamma^2}{2} + \frac{B_{\mathrm{b}}}{H_{\mathrm{b}}}\,\frac{Q_{\mathrm{b}}^2}{2} \tag{20}$$

where B_{b} and B_Γ are further material parameters. From Eq. (20), the evolution equations are computed as

$$\dot{\alpha}_\Gamma = \lambda^{\mathrm{b}}\,\partial_\Gamma\bar{\phi}^{\mathrm{b}} = -\lambda^{\mathrm{b}}\,(\frac{\mathrm{sign}(Y^N-\Gamma)}{S_2} + B_\Gamma\,\alpha_\Gamma) \tag{21}$$

$$\dot{\alpha}_{\mathrm{b}} = \lambda^{\mathrm{b}}\,\partial_{Q_{\mathrm{b}}}\bar{\phi}^{\mathrm{b}} = -\lambda^{\mathrm{b}}\,(1 + B_{\mathrm{b}}\,\alpha_{\mathrm{b}}) \tag{22}$$

$$\dot{D} = \lambda^{\mathrm{b}}\,\partial_Y\bar{\phi}^{\mathrm{b}} = \lambda^{\mathrm{b}}\,\frac{\mathrm{sign}(Y^N-\Gamma)}{S_2}\,N\,Y^{N-1}\ . \tag{23}$$

Clearly, brittle damage should evolve only in one half cycle (tension). This is enforced by allowing $\dot{D} > 0$ only, if $\mathrm{sign}(Y^{\mathrm{b}\,N} - \Gamma) \geq 0$, cf. (1). The model is completed by the classical Karush-Kuhn-Tucker conditions

$$\lambda^{\mathrm{b}} \geq 0\ , \quad \phi^{\mathrm{b}} \leq 0\ , \quad \lambda^{\mathrm{b}}\,\phi^{\mathrm{b}} = 0 \tag{24}$$

with λ^{b} being a consistency parameter.

Remark 2 *The proposed model shares some similarities with the well-known Paris law, cf. (4). Indeed, the Paris law describes fatigue crack growth characterized by three different regimes. An ultimate fatigue threshold, here represented by the initial threshold $Q_{\mathrm{b}0}$ and an evolving threshold Q_{b}, a regime of exponential fatigue crack growth, here controlled by the evolution of the internal variable Γ, and, finally, a regime of accelerated damage growth. For simulating the latter, the definitions*

$$\bar{\alpha}_{\Gamma\,\infty} := -\frac{sign(Y^N-\Gamma)}{S_2\,B_\Gamma}\ , \quad \bar{\alpha}_{\mathrm{b}\infty} := -\frac{1}{B_{\mathrm{b}}} \tag{25}$$

are inserted into Eq. (21) and Eq. (22) yielding

$$\dot{\alpha}_\Gamma = \lambda^{\mathrm{b}}\,B_\Gamma\,(\bar{\alpha}_{\Gamma\,\infty} - \alpha_\Gamma)\ , \quad \dot{\alpha}_{\mathrm{b}} = \lambda^{\mathrm{b}}\,B_{\mathrm{b}}\,(\bar{\alpha}_{\mathrm{b}\infty} - \alpha_{\mathrm{b}})\ . \tag{26}$$

Using these re-written evolution equations, the consistency parameter λ^{b} resulting from the consistency condition $\dot{\phi}^{\mathrm{b}} = 0$ is obtained as

$$\lambda^{\mathrm{b}} = \frac{\frac{sign(Y^N-\Gamma)}{S_2}\,N\,Y^{N-1}\,\dot{Y}}{B_\Gamma\,H_\Gamma\,\frac{sign(Y^N-\Gamma)}{S_2}\,(\alpha_\Gamma - \bar{\alpha}_{\Gamma\,\infty}) + B_{\mathrm{b}}\,H_{\mathrm{b}}\,(\alpha_{\mathrm{b}} - \bar{\alpha}_{\mathrm{b}\infty})}\ . \tag{27}$$

Consequently and in line with Paris law, the novel model shows also a regime of accelerated damage growth, i.e., $\lambda^{\mathrm{b}} \to \infty$ for $(\alpha_\Gamma, \alpha_{\mathrm{b}}) \to (\bar{\alpha}_{\Gamma\,\infty}, \bar{\alpha}_{\mathrm{b}\,\infty})$.

2.3 The coupled ductile-brittle damage model

In this section, the constitutive models summarized in Subsection 2.1 and Subsection 2.2 are combined yielding a coupled ductile-brittle model. Considering Eqs. (1), (2) and (16), the Helmholtz energy of that combined model reads

$$\begin{aligned}\Psi &= (1-D)\left(\frac{\boldsymbol{\epsilon}^{\mathrm{e}}:\mathbb{C}:\boldsymbol{\epsilon}^{\mathrm{e}}}{2}+H_{\mathrm{k}}\frac{||\boldsymbol{\alpha}_{\mathrm{k}}||^2}{2}+H_{\mathrm{i}}\frac{\alpha_{\mathrm{i}}^2}{2}\right)+H_{\Gamma}\,\frac{\alpha_{\Gamma}^2}{2}+H_{\mathrm{b}}\,\frac{\alpha_{\mathrm{b}}^2}{2}\\ &= (1-D)\,Y+H_{\Gamma}\,\frac{\alpha_{\Gamma}^2}{2}+H_{\mathrm{b}}\,\frac{\alpha_{\mathrm{b}}^2}{2}\ .\end{aligned}\tag{28}$$

It is completed by assuming an additive decomposition of damage $D\in[0,D_{\mathrm{crit}}]$ into the different parts parts, i.e.,

$$D=\gamma^{\mathrm{p}}\,D^{\mathrm{p}}+\gamma^{\mathrm{b}}\,D^{\mathrm{b}}\ ,\quad\text{with}\quad\gamma^{\mathrm{b}}:=1-\gamma^{\mathrm{p}},\tag{29}$$

where γ^{p} and γ^{b} are the corresponding composition factors. Conform to the previous subsections, the superscripts $(\bullet)^{\mathrm{p}}$ and $(\bullet)^{\mathrm{b}}$ indicate variables associated with the plasticity-governed ductile damage model (see Subsection 2.1) and those related to quasi-brittle damage accumulation (see Subsection 2.2). With assumption (29), the driving forces governing ductile and brittle material degradation are given by

$$Y^{\mathrm{p}}=-\partial_{D^{\mathrm{p}}}\Psi=\gamma^{\mathrm{p}}\,Y\quad\text{and}\quad Y^{\mathrm{b}}=-\partial_{D^{\mathrm{b}}}\Psi=\gamma^{\mathrm{b}}\,Y\ .\tag{30}$$

and the evolution equations (13) and (23) are eventually recast as

$$\dot{D}^{\mathrm{p}}=p\,\frac{{Y^{\mathrm{p}}}^{M-1}}{S_1},\quad\dot{D}^{\mathrm{b}}=\lambda^{\mathrm{b}}\,\frac{\operatorname{sign}({Y^{\mathrm{b}}}^{N}-\Gamma)}{S_2}\,N\,{Y^{\mathrm{b}}}^{N-1}\tag{31}$$

where $D^{\mathrm{p}}\in[0,D^{\mathrm{p}}_{\mathrm{crit}}]$ and $D^{\mathrm{b}}\in[0,D^{\mathrm{b}}_{\mathrm{crit}}]$.

Remark 3 *The composition factor γ^{p} will be regarded as a constant material parameter in what follows. Even though this seems to be a simplifying assumption, recent experiments on flat sheets of Al2024 have shown that this parameter is almost direction-independent which suggests the overall practical relevance of $\gamma^{\mathrm{p}}=$ const. Nevertheless, a variable composition factor, i.e., for defining a different amount of brittleness for different applied strain ranges, could also be considered. In this case, the algorithm would be in fact more complex distracting from the main focus of the present expositions.*

3 A variationally consistent formulation of the ductile-brittle damage model – the time-continuous problem

In the present section, the ductile-brittle damage model discussed previously is reformulated into a variationally consistent format. Within the resulting approach, all state variables follow naturally and conveniently from minimizing the stress power of the solid. Due to the underlying variational basis, such models are referred to as *variational constitutive updates*, cf. (6; 7; 10–13). Although such updates show significant advantages compared to conventional material descriptions (see (6; 7; 13)), they have only been developed for relatively simple constitutive models yet, cf. (6; 7; 9–13). By way of contrast,

a variational formulation of the complex constitutive model summarized in the previous section is elaborated here.

For introducing some notations and for explaining the underlying ideas, ideal elastoplasticity is considered first (Subsection 3.1). Subsequently, the ductile model (Subsection 3.2) and the brittle damage model (Subsection 3.3) are detailed. Finally, some comments concerning the coupling of those models are given in Subsection 3.4.

3.1 Associative ideal elastoplasticity

Neglecting ductile damage accumulation as well as hardening effects, the model described in Subsection 2.1 simplifies to that of ideal elastoplasticity. In this case, the Helmholtz energy is given by

$$\Psi = \frac{1}{2}\,\boldsymbol{\epsilon}^{\mathrm{e}} : \mathbb{C} : \boldsymbol{\epsilon}^{\mathrm{e}} \ , \tag{32}$$

the yield function reads

$$\phi^{\mathrm{p}}(\boldsymbol{\sigma}) = \underbrace{\sqrt{\frac{3}{2}\,\mathrm{dev}(\boldsymbol{\sigma}) : \mathrm{dev}(\boldsymbol{\sigma})}}_{=:\,\sigma_{\mathrm{eq}}} - Q_0^{\mathrm{eq}} \leq 0 \tag{33}$$

and the flow rule yields

$$\dot{\boldsymbol{\epsilon}}^{\mathrm{p}} = \lambda\,\partial_{\boldsymbol{\sigma}}\phi^{\mathrm{p}} \ . \tag{34}$$

Accordingly, the flow rule is associative and thus, it can be derived from the canonical postulate of maximum dissipation, i.e.,

$$\sup_{\boldsymbol{\sigma},\phi^{\mathrm{p}}\leq 0} \mathcal{D} \quad \Rightarrow \quad \dot{\boldsymbol{\epsilon}}^{\mathrm{p}} = \lambda\,\partial_{\boldsymbol{\sigma}}\phi^{\mathrm{p}} \ . \tag{35}$$

By introducing the characteristic function of the space of admissible stresses $\mathbb{E}_{\boldsymbol{\sigma}} := \{\boldsymbol{\sigma}\,|\,\phi^{\mathrm{p}} \leq 0\}$ as

$$J(\boldsymbol{\sigma}) := \begin{cases} 0 & \forall \boldsymbol{\sigma} \in \mathbb{E}_{\boldsymbol{\sigma}} \\ \infty & \text{otherwise} \ , \end{cases} \tag{36}$$

this principle can be re-written into the mathematically more abstract format

$$\sup_{\boldsymbol{\sigma}}\{\mathcal{D} + J\} := J^* \quad \Rightarrow \quad \dot{\boldsymbol{\epsilon}}^{\mathrm{p}} \in \partial J \ . \tag{37}$$

Following standard notations used in convex analysis (see (28)), ∂J denotes the subdifferential of J. A careful analysis of Eq. (37) reveals the physical interpretation of the newly introduced variable J^*: Provided that the flow rule is associative and the stresses are admissible ($\boldsymbol{\sigma} \in \mathbb{E}_{\boldsymbol{\sigma}}$), J^* is the dissipation. Furthermore, since $\boldsymbol{\sigma}$ and $\dot{\boldsymbol{\epsilon}}^{\mathrm{p}}$ are energetically conjugate to one another ($\boldsymbol{\sigma} = -\partial_{\boldsymbol{\epsilon}^{\mathrm{p}}}\Psi$), J^* is the Legendre-Fenchel transform of J, cf. (28). As such, J^* depends only on the plastic strain rates and is independent of the stresses. The derivation of closed-form solutions for J^* is usually not straightforward. Fortunately, if the equivalent stress measure σ_{eq} is positively homogeneous of degree one (see Eq. (33)), Euler's theorem can be applied resulting in $\sigma_{\mathrm{eq}} = \partial_{\boldsymbol{\sigma}}\sigma_{\mathrm{eq}} : \boldsymbol{\sigma}$. With this identity, the closed form solution for J^* yields

$$J^*(\dot{\boldsymbol{\epsilon}}^{\mathrm{p}}) = \begin{cases} \lambda\, Q_0^{\mathrm{eq}} & \forall \boldsymbol{\sigma} \in \mathbb{E}_{\boldsymbol{\sigma}} \wedge \forall \dot{\boldsymbol{\epsilon}}^{\mathrm{p}} \in \partial J \\ \infty & \text{otherwise} \ . \end{cases} \tag{38}$$

The aforementioned points have already highlighted the importance of the functional J^*. However, its probably most important property becomes obvious, if J^* is inserted into the stress power $\mathcal{P}$ leading to

$$\mathcal{P} := \boldsymbol{\sigma} : \dot{\boldsymbol{\epsilon}} = \dot{\Psi}(\dot{\boldsymbol{\varepsilon}}, \dot{\boldsymbol{\varepsilon}}^{\mathrm{p}}) + J^*(\dot{\boldsymbol{\varepsilon}}^{\mathrm{p}}) \ . \tag{39}$$

As shown, e.g., in (6; 7; 9–13), potential (39) provides a variational basis for associative plasticity theory. More explicitly,

$$\dot{\boldsymbol{\epsilon}}^{\mathrm{p}} = \arg\inf_{\dot{\boldsymbol{\epsilon}}^{\mathrm{p}}} \{\dot{\Psi}(\dot{\boldsymbol{\varepsilon}}, \dot{\boldsymbol{\varepsilon}}^{\mathrm{p}}) + J^*(\dot{\boldsymbol{\varepsilon}}^{\mathrm{p}})\} := \mathcal{P}^{\mathrm{red}}, \qquad \boldsymbol{\sigma} = \partial_{\dot{\boldsymbol{\epsilon}}} \mathcal{P}^{\mathrm{red}}. \tag{40}$$

As a consequence, the internal variables follow naturally from minimizing the stress power which acts, in turn, as a hyperelastic potential defining the stress response. Clearly, in contrast to conventional hyperelasticity, potential (40) is incremental in nature, i.e., it evolves in time. Since minimization principle (40) is not standard, its consistency has to be proved. Thereby, the nonlinear constraint $\dot{\boldsymbol{\epsilon}}^{\mathrm{p}} \in \partial J$ is crucial. For defining a flow direction complying with $\dot{\boldsymbol{\epsilon}}^{\mathrm{p}} \in \partial J$, Lagrange factors were introduced in (6; 7). Owing to the simplicity of the constitutive models in (6; 7), such factors could be computed analytically. Clearly, such a method is very elegant. Unfortunately, it cannot be extended in a straightforward manner to more complex constitutive models. By way of contrast, only the plastic multipliers were considered as unknowns in the minimization problem in (10), while the flow direction was enforced by considering a residual similar to that in a classical return-mapping scheme. Thus, the respective algorithm is a constrained minimization problem. A general framework yielding an unconstrained minimization principle was recently proposed in (9; 13). In contrast to (6; 7; 10), the flow direction is enforced by using a suitable parameterization. One such parameterization was discussed in (9; 13). It is based on so-called *pseudo stresses*. Here an alternative, more efficient method is proposed. Importantly, this parameterization can be conveniently discretized leading to an effective numerical implementation.

Considering a von Mises-type flow rule, the nonlinear constraint $\dot{\boldsymbol{\epsilon}}^{\mathrm{p}} \in \partial J$ can be directly enforced by a suitable parameterization of the set of admissible plastic flows $\mathbb{E}_{\boldsymbol{\epsilon}^{\mathrm{p}}}$ defined as

$$\dot{\boldsymbol{\epsilon}}^{\mathrm{p}} \in \{\boldsymbol{A} \in \mathbb{R}^{3\times 3} \mid \boldsymbol{A} = \boldsymbol{A}^T, \ \mathbf{1} : \boldsymbol{A} = \mathbf{0}\} =: \mathbb{E}_{\boldsymbol{\epsilon}^{\mathrm{p}}} \ . \tag{41}$$

The symmetry condition, together with the deviatoric constraint, define a five-dimensional solution space. For spanning it, two different parameterizations will be considered here:

- Direct parameterization:

$$\dot{\boldsymbol{\epsilon}}^{\mathrm{p}} = \begin{bmatrix} \dot{\epsilon}^{\mathrm{p}}_{11} & \dot{\epsilon}^{\mathrm{p}}_{12} & \dot{\epsilon}^{\mathrm{p}}_{13} \\ \dot{\epsilon}^{\mathrm{p}}_{12} & \dot{\epsilon}^{\mathrm{p}}_{22} & \dot{\epsilon}^{\mathrm{p}}_{23} \\ \dot{\epsilon}^{\mathrm{p}}_{13} & \dot{\epsilon}^{\mathrm{p}}_{23} & -\dot{\epsilon}^{\mathrm{p}}_{11} - \dot{\epsilon}^{\mathrm{p}}_{22} \end{bmatrix} \tag{42}$$

- Indirect parameterization by using a projection:

$$\dot{\boldsymbol{\epsilon}}^{\mathrm{p}} = \mathbb{P}_{\mathrm{dev}} : \mathbf{m}, \qquad \mathbf{m} = \mathbf{m}^T \ , \text{ but } \mathbf{m} : \mathbf{1} \neq 0. \tag{43}$$

For proving consistency of minimization principle (40), the indirect parameterization is employed here. By inserting $\lambda = \sqrt{2/3}\ ||\dot{\boldsymbol{\epsilon}}^{\mathrm{p}}||$ into the stress power (39), the gradient

$$\frac{\partial \mathcal{P}}{\partial \mathbf{m}} = \frac{\partial \mathcal{P}}{\partial \dot{\boldsymbol{\epsilon}}^{\mathrm{p}}} : \mathbb{P}_{\mathrm{dev}} = -\mathrm{dev}(\boldsymbol{\sigma}) + \sqrt{\frac{2}{3}}\, Q_0^{\mathrm{eq}}\, \frac{\dot{\boldsymbol{\epsilon}}^{\mathrm{p}}}{||\dot{\boldsymbol{\epsilon}}^{\mathrm{p}}||} \tag{44}$$

can be computed. Clearly, stationarity of $\mathcal{P}$ requires that this gradient vanishes for plastic loading. This implies

$$\dot{\boldsymbol{\epsilon}}^{\mathrm{p}} = \sqrt{\frac{3}{2}}\,||\dot{\boldsymbol{\epsilon}}^{\mathrm{p}}||\,\frac{\mathrm{dev}(\boldsymbol{\sigma})}{Q_0^{\mathrm{eq}}}. \tag{45}$$

Using the identities $\lambda = \sqrt{2/3}\;||\dot{\boldsymbol{\epsilon}}^{\mathrm{p}}||$ and $\phi^{\mathrm{p}} = 0$, the equivalence between stationarity condition Eq. (45) and the classical flow rule (34) becomes obvious.

Finally, it will be shown that in addition to the flow rule, the yield function is also consistently enforced via the variational problem (40). For that purpose, the stability condition of the stress power

$$\frac{\partial \mathcal{P}}{\partial \mathbf{m}} : \boldsymbol{A} \geq 0 \qquad \forall \boldsymbol{A} \in \mathbb{E}_{\boldsymbol{\epsilon}^{\mathrm{p}}} \tag{46}$$

is evaluated for the admissible choice $\boldsymbol{A} = \dot{\boldsymbol{\epsilon}}^{\mathrm{p}}$. A straightforward computation yields

$$\frac{\partial \mathcal{P}}{\partial \mathbf{m}} : \boldsymbol{A} = \sqrt{\frac{2}{3}}\,||\dot{\boldsymbol{\epsilon}}^{\mathrm{p}}||\;[-\sigma_{\mathrm{eq}} + Q_0^{\mathrm{eq}}] = -\sqrt{\frac{2}{3}}\,||\dot{\boldsymbol{\epsilon}}^{\mathrm{p}}||\;\phi^{\mathrm{p}} \geq 0 \;\Leftrightarrow\; \phi^{\mathrm{p}} \leq 0\;. \tag{47}$$

Accordingly, any stable configuration regarding the stress power is characterized by admissible stresses ($\phi^{\mathrm{p}} \leq 0$). Therefore, variational principle (40) is indeed consistent with the underlying constitutive assumptions. Analogously to hyperelasticity, the admissible stresses can be computed as $\boldsymbol{\sigma} = \partial_{\dot{\boldsymbol{\epsilon}}} \inf_{\mathbf{m}} \mathcal{P}$.

3.2 The ductile damage model

Next, the ductile damage model is reformulated into a variationally consistent form. It bears emphasis that the respective evolution equations defining the internal variables are not associative anymore. Consequently, this model does not fulfill the postulate of maximum dissipation. However, it is possible to define an extended variational minimization principle complying with this structure. In line with (9; 26), the underlying idea is similar to that presented within the previous subsection, i.e., the stress power of the solid is minimized. However, the non-associative evolution equations are a priori enforced by using the aforementioned parameterization of the flow rule. Mathematically speaking, this can be interpreted as a constrained minimization problem in which the respective constraints have already been explicitly inserted.

For computing the stress power of the ductile damage model discussed in Subsection 2.1, the dissipation as well as the rate of the Helmholtz energy are required. Considering Eq. (3), Eq. (8) and Eqs. (10)–(13), the dissipation can be computed as

$$\mathcal{D} = \lambda^{\mathrm{p}}\, Q_0^{\mathrm{eq}} + \lambda^{\mathrm{p}}\,(B_{\mathrm{k}}\, H_{\mathrm{k}}\, \boldsymbol{\alpha}_{\mathrm{k}} : \boldsymbol{\alpha}_{\mathrm{k}} + B_{\mathrm{i}}\, H_{\mathrm{i}}\, \alpha_{\mathrm{i}}^2) + Y\,\dot{D}\;, \tag{48}$$

while the rate of the Helmholtz energy yields

$$\begin{aligned} \dot{\Psi} = \;& \boldsymbol{\sigma} : \dot{\boldsymbol{\epsilon}} - \dot{D}\,Y - \lambda^{\mathrm{p}}\,\left(\tilde{\boldsymbol{\sigma}} - \tilde{\boldsymbol{Q}}_{\mathrm{k}}\right) : \partial_{\tilde{\boldsymbol{\sigma}}}\phi^{\mathrm{p}} \\ & -\lambda^{\mathrm{p}}\,\left[B_{\mathrm{k}}\, H_{\mathrm{k}}\, \boldsymbol{\alpha}_{\mathrm{k}} : \boldsymbol{\alpha}_{\mathrm{k}} + B_{\mathrm{i}}\, H_{\mathrm{i}}\, \alpha_{\mathrm{i}}^2 - \tilde{Q}_{\mathrm{i}}\right]\;. \end{aligned} \tag{49}$$

Accordingly, the stress power is given by

$$\mathcal{P} = \boldsymbol{\sigma} : \dot{\boldsymbol{\epsilon}} - \lambda^{\mathrm{p}}\,\left(\tilde{\boldsymbol{\sigma}} - \tilde{\boldsymbol{Q}}_{\mathrm{k}}\right) : \partial_{\tilde{\boldsymbol{\sigma}}}\phi^{\mathrm{p}} + \lambda^{\mathrm{p}}\,\left(Q_0^{\mathrm{eq}} + \tilde{Q}_{\mathrm{i}}\right)\;. \tag{50}$$

Following the previous subsection, the stress power is parameterized by the flow rule, i.e., $\mathbf{m}$ represents the independent variable defining the rate of the internal variables (see Eq. (43)). For instance, the plastic multiplier as a function in terms of $\dot{\boldsymbol{\epsilon}}^{\mathrm{p}}$ reads

$$\lambda^{\mathrm{p}} = \sqrt{\frac{2}{3}}\,(1-D)\,||\mathbb{P}_{\mathrm{dev}} : \mathbf{m}|| \ . \tag{51}$$

By inserting this parameterization into Eq. (50), the stress power is re-written as

$$\begin{aligned}\mathcal{P} = \mathcal{P}(\dot{\boldsymbol{\epsilon}}, \dot{\boldsymbol{\epsilon}}^{\mathrm{p}}(\mathbf{m})) = \ & \boldsymbol{\sigma} : \dot{\boldsymbol{\epsilon}} - (1-D)\,\left(\tilde{\boldsymbol{\sigma}} - \tilde{\boldsymbol{Q}}_{\mathrm{k}}\right) : \dot{\boldsymbol{\epsilon}}^{\mathrm{p}} \\ & + \sqrt{\frac{2}{3}}\,(1-D)\,||\dot{\boldsymbol{\epsilon}}^{\mathrm{p}}||\,\left(Q_0^{\mathrm{eq}} + \tilde{Q}_{\mathrm{i}}\right) \ .\end{aligned} \tag{52}$$

Clearly, in case of plastic loading, energy stationarity requires

$$\frac{\partial \mathcal{P}}{\partial \mathbf{m}} = -(1-D)\,\left[\left(\mathrm{dev}(\tilde{\boldsymbol{\sigma}}) - \tilde{\boldsymbol{Q}}_{\mathrm{k}}\right) - \sqrt{\frac{2}{3}}\,\left(Q_0^{\mathrm{eq}} + \tilde{Q}_{\mathrm{i}}\right)\,\frac{\dot{\boldsymbol{\epsilon}}^{\mathrm{p}}}{||\dot{\boldsymbol{\epsilon}}^{\mathrm{p}}||}\right] = \mathbf{0} \ . \tag{53}$$

This condition is fulfilled, if and only if

$$\dot{\boldsymbol{\epsilon}}^{\mathrm{p}} = \sqrt{\frac{3}{2}}\,||\dot{\boldsymbol{\epsilon}}^{\mathrm{p}}||\,\frac{\mathrm{dev}(\tilde{\boldsymbol{\sigma}}) - \tilde{\boldsymbol{Q}}_{\mathrm{k}}}{Q_0^{\mathrm{eq}} + \tilde{Q}_{\mathrm{i}}} \ . \tag{54}$$

By inserting the necessary condition for yielding $\phi^{\mathrm{p}} = 0$ into Eq. (54), it can be seen that the flow rule (54) implied by the variational principle $\inf_{\dot{\boldsymbol{\epsilon}}} \mathcal{P}$ is equivalent to that of the underlying model, cf. Eq. (10). Furthermore, analyzing the stability condition (46) in the direction of $\dot{\boldsymbol{\epsilon}}^{\mathrm{p}}$ proves that the resulting stresses are admissible, i.e.,

$$\frac{\partial \mathcal{P}}{\partial \mathbf{m}} : \dot{\boldsymbol{\epsilon}}^{\mathrm{p}} = -\sqrt{\frac{2}{3}}\,(1-D)\,||\dot{\boldsymbol{\epsilon}}^{\mathrm{p}}||\,\phi^{\mathrm{p}} \geq 0 \quad \Leftrightarrow \quad \phi^{\mathrm{p}} \leq 0 \ . \tag{55}$$

Consequently and fully analogously to the associative model, the variational principle $\inf \mathcal{P}$ contains the flow rule (and thus, the evolution equations as well) and the yield function. Having solved the minimization problem $\inf \mathcal{P}$, the rate of damage evolution can be computed subsequently (see Eq. (13)) and the stresses follow from the hyperelastic-type relation $\boldsymbol{\sigma} = \partial_{\dot{\boldsymbol{\epsilon}}} \inf_{\mathbf{m}} \mathcal{P}$.

3.3 The brittle damage model

Having presented the variational structure of the ductile damage model, focus is now on the quasi-brittle counterpart. In contrast to the material law discussed in the previous section, the failure function ϕ^{b} is not positively homogeneous of degree one. Thus, Euler's theorem cannot be applied which was crucial for the derivations in the last subsection. However, a similar procedure can also be applied in case of the quasi-brittle damage model.

Following Subsection 3.2, the stress power is considered. For that purpose, the dissipation and the rate of the Helmholtz energy are required. Using Eqs. (16), (17), (18), (19) and (21)–(23) they result in

$$\mathcal{D} = \lambda^{\mathrm{b}}\,\left[Q_{\mathrm{b}0} + (N-1)\,Y^N\,\frac{\mathrm{sign}(Y^N - \Gamma)}{S_2} + B_\Gamma\,H_\Gamma\,\alpha_\Gamma^2 + B_{\mathrm{b}}\,H_{\mathrm{b}}\,\alpha_{\mathrm{b}}^2\right] \tag{56}$$

and

$$\dot{\Psi} = -\lambda^{\mathrm{b}} \Big[N\, Y^N\, \frac{\mathrm{sign}(Y^N - \Gamma)}{S_2} - \Gamma\, \frac{\mathrm{sign}(Y^N - \Gamma)}{S_2} \\ -Q_{\mathrm{b}} + B_\Gamma\, H_\Gamma\, \alpha_\Gamma^2 + B_{\mathrm{b}}\, H_{\mathrm{b}}\, \alpha_{\mathrm{b}}^2 \Big] \ . \tag{57}$$

Consequently, by combining these equations, the stress power reads

$$\mathcal{P} = -\lambda^{\mathrm{b}} \left[\frac{|Y^N - \Gamma|}{S_2} - (Q_{\mathrm{b}0} + Q_{\mathrm{b}}) \right] = -\lambda^{\mathrm{b}}\, \phi^{\mathrm{b}} \ . \tag{58}$$

Accordingly, stability of the stress power $\mathcal{P} = \mathcal{P}(\lambda^{\mathrm{b}})$ leads to

$$\inf_{\lambda^{\mathrm{b}}} \mathcal{P} \quad \Rightarrow \quad \frac{\partial \mathcal{P}}{\partial \lambda^{\mathrm{b}}} = -\phi^{\mathrm{b}} \geq 0 \quad \Leftrightarrow \quad \phi^{\mathrm{b}} \leq 0 \ . \tag{59}$$

Hence, principle $\inf \mathcal{P}$ is indeed a variational reformulation of the material law discussed in Subsection 2.2. As within the previously described models, the stresses follow from the hyperelastic-type relation $\boldsymbol{\sigma} = \partial_{\boldsymbol{\epsilon}} \inf_{\lambda^{\mathrm{b}}} \mathcal{P}$.

3.4 The coupled ductile-brittle damage model

For capturing the damage processes observed in high-strength aluminum alloys, both variational schemes addressed in Subsections 3.2 and 3.3 have to be coupled. Accordingly, a monolithic, extended minimization problem could be formulated. However, that principle would not be ideal from a computational point of view, since its numerical complexity would be higher than the sum of the two subproblems considered alone. For this reason, a staggered scheme will be used. Clearly, if an arbitrary coupled mechanical problem is decomposed into subproblems, the resulting numerical approach shows often some drawbacks. A typical examples is given by the thermomechanically coupled theory of finite strain plasticity theory, cf. (29). Although the purely mechanical subproblem as well as that related to the temperature are stable, the overall algorithm is only conditionally stable, see (30). Fortunately, due the additive structure of the Helmholtz energy (28) and the linearity of the stress power with respect to the rate of the internal variables, the minimization principle $\inf \mathcal{P}$ can be consistently uncoupled. More explicitly, the dissipation of the coupled problem decomposes additively into the two parts related to the purely ductile damage model and that of the quasi-brittle model, i.e.,

$$\mathcal{D} = \underbrace{\left(\dot{D}^{\mathrm{p}}\, Y - (1 - D)\, \dot{Y} \right)}_{=\mathcal{D}^{\mathrm{p}}(\dot{\boldsymbol{\epsilon}}^{\mathrm{p}})} + \underbrace{\left(\dot{D}^{\mathrm{b}}\, Y + \overline{H_\Gamma\, \frac{\alpha_\Gamma^2}{2} + H_{\mathrm{b}}\, \frac{\alpha_{\mathrm{b}}^2}{2}}^{\cdot} \right)}_{=\mathcal{D}^{\mathrm{b}}(\lambda^{\mathrm{b}})} \ . \tag{60}$$

The same holds also for the rate of the Helmholtz energy, since $\dot{\Psi} = \boldsymbol{\sigma} : \dot{\boldsymbol{\epsilon}} - \mathcal{D}$. For this reason, the solution of the fully coupled problem can be computed by ignoring quasi-brittle damage accumulation first. Subsequently, a purely quasi-brittle-type loading is considered.

Remark 4 *The monolithic, fully coupled variational principle describing the ductile-brittle damage model can be written as*

$$(\lambda^{\mathrm{b}}, \mathbf{m}) = \mathit{arg} \inf_{\lambda^{\mathrm{b}}, \mathbf{m}} \mathcal{P} \quad \mathit{and} \quad \boldsymbol{\sigma} = \partial_{\boldsymbol{\epsilon}} \inf_{\lambda^{\mathrm{b}}, \mathbf{m}} \mathcal{P} \ . \tag{61}$$

By setting the composition factor $\gamma^{\mathrm{p}} = 1$, the ductile model is obtained, while $\gamma^{\mathrm{b}} = 1$ is associated with the purely quasi-brittle model, cf. Eq. (29). Interestingly, if energy minimization is the overriding principle, the extended variational principle

$$(\lambda^{\mathrm{b}}, \mathbf{m}, \gamma^{\mathrm{p}}) = arg \inf_{\lambda^{\mathrm{b}}, \mathbf{m}, \gamma^{\mathrm{p}}} \mathcal{P} \quad and \quad \boldsymbol{\sigma} = \partial_{\dot{\boldsymbol{\epsilon}}} \inf_{\lambda^{\mathrm{b}}, \mathbf{m}, \gamma^{\mathrm{p}}} \mathcal{P} \tag{62}$$

could be also considered. By doing so, the interaction between the different damage mechanisms would evolve during deformation. Such a promising extended model which is beyond the scope of the present paper will be discussed in detail in a future work.

4 Numerical implementation - Variational constitutive updates

In the previous section, a variational principle for the coupled ductile-brittle damage model was proposed. Here, this principle is discretized by a suitable time discretization yielding an effective numerical update scheme. Within this scheme, all unknown variables at a certain time step can be computed by minimizing the integrated stress power. Following the structure of Section 3, ideal plasticity is considered first (see Subsection 4.1). Subsequently, variational updates are elaborated for the ductile damage law (Subsection 4.2) as well as for the quasi-brittle damage (Subsection 4.3). Finally, the complete algorithm is discussed in Subsection 4.4.

4.1 Associative ideal elastoplasticity

For explaining the underlying idea of variational constitutive updates, focus is on associative ideal elastoplasticity first. Within a continuous time frame, the variational update has already been discussed in Subsection 3.1. Here, this variational principle is integrated yielding the discrete counterpart

$$I_{\mathrm{inc}} := \int_{t_n}^{t_{n+1}} \mathcal{P}\, \mathrm{d}t = \int_{t_n}^{t_{n+1}} [\dot{\Psi} + \lambda\, Q_0^{\mathrm{eq}}]\, \mathrm{d}t = \Psi_{n+1} - \Psi_n + \Delta\lambda\, Q_0^{\mathrm{eq}}\,, \tag{63}$$

with $\Delta\lambda := \int_{t_n}^{t_{n+1}} \lambda\, \mathrm{d}t$. Clearly, the state variables at the previous time step t_n are known. Consequently, by assuming a conventional displacement-driven discretization technique such as the finite element method, the only unknowns in Eq. (63) are the plastic multiplier $\Delta\lambda$ and the plastic strains at time t_{n+1}. Thus, applying a backward Euler time integration, i.e.,

$$\Delta\boldsymbol{\epsilon}^{\mathrm{p}} := \boldsymbol{\epsilon}^{\mathrm{p}}_{n+1} - \boldsymbol{\epsilon}^{\mathrm{p}}_{n} = \mathbb{P}_{\mathrm{dev}} : \Delta\mathbf{m}, \quad \Delta\lambda(\Delta\mathbf{m}) = \sqrt{\frac{2}{3}}\, ||\mathbb{P}_{\mathrm{dev}} : \Delta\mathbf{m}|| \tag{64}$$

leads to the optimization problem

$$\Delta\mathbf{m} = \arg\inf I_{\mathrm{inc}}(\Delta\mathbf{m}). \tag{65}$$

As evident from Eq. (64), the physical constraint $\Delta\boldsymbol{\epsilon}^{\mathrm{p}} : \mathbf{1}$ has been enforced by the projection method (43). Consistency of the algorithm (65) can be proved in a relatively simple manner. More explicitly, the gradient of I_{inc} can be computed as

$$\frac{\partial I_{\mathrm{inc}}}{\partial \Delta\mathbf{m}} = \frac{\partial I_{\mathrm{inc}}}{\partial \boldsymbol{\epsilon}^{\mathrm{p}}_{n+1}} : \mathbb{P}_{\mathrm{dev}} = -\mathrm{dev}(\boldsymbol{\sigma}_{n+1}) + \sqrt{\frac{2}{3}}\, Q_0^{\mathrm{eq}}\, \frac{\Delta\boldsymbol{\epsilon}^{\mathrm{p}}}{||\Delta\boldsymbol{\epsilon}^{\mathrm{p}}||}\,. \tag{66}$$

Following the same argumentation as explained in detail in Subsection 3.1, Eq. (66) implies the discrete flow rule

$$\Delta\boldsymbol{\epsilon}^{\mathrm{p}} = \sqrt{\frac{3}{2}}\,||\Delta\boldsymbol{\epsilon}^{\mathrm{p}}||\,\frac{\mathrm{dev}(\boldsymbol{\sigma}_{n+1})}{Q_0^{\mathrm{eq}}} \tag{67}$$

and the stability condition

$$\frac{\partial I_{\mathrm{inc}}}{\partial\Delta\mathbf{m}} : \Delta\boldsymbol{\epsilon}^{\mathrm{p}} = -\sqrt{\frac{2}{3}}\,||\Delta\boldsymbol{\epsilon}^{\mathrm{p}}||\,\phi^{\mathrm{p}}_{n+1} \geq 0 \quad \Leftrightarrow \quad \phi^{\mathrm{p}}_{n+1} \leq 0\ . \tag{68}$$

As a result, the variational update (65) is consistent. More explicitly, it implies a first-order approximation of the flow rule and physically inadmissible stress states are naturally excluded. Having updated the internal variables, the stresses can be computed as

$$\boldsymbol{\sigma}_{n+1} = \partial_{\boldsymbol{\epsilon_{n+1}}} \inf_{\Delta\mathbf{m}} I_{\mathrm{inc}}\ . \tag{69}$$

Remark 5 *The presented variational constitutive update depends, in addition to the underlying constitutive model, also on the employed time integration scheme. According to Eq. (64), the backward Euler integration scheme has been applied here. However, other consistent integration schemes can also be used.*

4.2 The ductile damage model

4.2.1 Fundamentals

By combining Eq. (48) with the definition of the Helmholtz energy $\Psi = (1-D)\,Y$, the variational principle characterizing the ductile damage model can be written as

$$\mathbf{m} = \arg\inf_{\mathbf{m}} \mathcal{P}, \quad \mathcal{P} := (1-D)\,\dot{Y} + \lambda^{\mathrm{p}}\left[Q_0^{\mathrm{eq}} + B_{\mathrm{k}}\,H_{\mathrm{k}}\,\boldsymbol{\alpha}_{\mathrm{k}} : \boldsymbol{\alpha}_{\mathrm{k}} + B_{\mathrm{i}}\,H_{\mathrm{i}}\,\alpha_{\mathrm{i}}^2\right]. \tag{70}$$

In addition to the rates of the plastic strains ($\dot{\boldsymbol{\epsilon}}^{\mathrm{p}} = \mathbb{P}_{\mathrm{dev}} : \mathbf{m}$), the remaining state variables are kept fixed within the minimization problem (70), cf. (7; 11). Hence, it can be replaced by the alternative variational principle

$$\mathbf{m} = \arg\inf_{\mathbf{m}} \tilde{\mathcal{P}}\ , \qquad \tilde{\mathcal{P}} := \dot{Y} + p\,\left[Q_0^{\mathrm{eq}} + B_{\mathrm{k}}\,H_{\mathrm{k}}\,\boldsymbol{\alpha}_{\mathrm{k}} : \boldsymbol{\alpha}_{\mathrm{k}} + B_{\mathrm{i}}\,H_{\mathrm{i}}\,\alpha_{\mathrm{i}}^2\right]\ . \tag{71}$$

where the substitution $p = \lambda^{\mathrm{p}}/(1-D)$ has been applied. The advantage of Eq. (71) compared to Eq. (70) is that the functional $\tilde{\mathcal{P}}$ does not depend on the damage variable D anymore – at least not explicitly. For this reason, D can be computed in a post-processing step leading to an efficient numerical formulation.

For deriving an efficient numerical formulation, a backward Euler integration is employed resulting in

$$\begin{aligned} I_{\mathrm{inc}} =& \int_{t_n}^{t_{n+1}} \tilde{\mathcal{P}}\,\mathrm{d}t \\ =& Y_{n+1} - Y_n + \sqrt{\tfrac{2}{3}}\,||\Delta\boldsymbol{\epsilon}^{\mathrm{p}}||\left[Q_0^{\mathrm{eq}} + (B_{\mathrm{k}}\,H_{\mathrm{k}}\,||\boldsymbol{\alpha}_{\mathrm{k}\,n+1}||^2 + B_{\mathrm{i}}\,H_{\mathrm{i}}\,\alpha^2_{\mathrm{i}\,n+1})\right]\ . \end{aligned} \tag{72}$$

The same time integration scheme is also applied to the evolution equations and the flow rule, i.e.,

$$\begin{aligned} \Delta\boldsymbol{\epsilon}^{\mathrm{p}} = \boldsymbol{\epsilon}^{\mathrm{p}}_{n+1} - \boldsymbol{\epsilon}^{\mathrm{p}}_{n} &= \mathbb{P}_{\mathrm{dev}} : \Delta\mathbf{m}\ , \\ \boldsymbol{\alpha}_{\mathrm{k}\,n+1} &= \frac{\boldsymbol{\alpha}_{\mathrm{k}\,n} - \Delta\boldsymbol{\epsilon}^{\mathrm{p}}}{1 + B_{\mathrm{k}}\sqrt{\frac{2}{3}}\,||\Delta\boldsymbol{\epsilon}^{\mathrm{p}}||}\ , \quad \alpha_{\mathrm{i}\,n+1} = \frac{\alpha_{\mathrm{i}\,n} - \sqrt{\frac{2}{3}}\,||\Delta\boldsymbol{\epsilon}^{\mathrm{p}}||}{1 + B_{\mathrm{i}}\sqrt{\frac{2}{3}}||\Delta\boldsymbol{\epsilon}^{\mathrm{p}}||}\ . \end{aligned} \tag{73}$$

With this approximation, the variational constitutive update is obtained as

$$\Delta\mathbf{m} = \arg\inf_{\Delta\mathbf{m}} I_{\mathrm{inc}}. \tag{74}$$

Having computed the solution of Eq. (74), the update of the damage variable follows from the first-order approximation of Eq. $(15)_4$ yielding

$$D_{n+1} = D_n + \sqrt{\frac{2}{3}}\,||\Delta\boldsymbol{\epsilon}^{\mathrm{p}}||\,\frac{Y^{M-1}_{n+1}}{S_1}\ . \tag{75}$$

4.2.2 Consistency of the algorithm

For proving consistency of the variational constitutive update (71), it has to be shown that it implies the flow rule (54) as well as the yield function ($\phi^{\mathrm{p}} \leq 0$), if $\Delta t = t_{n+1} - t_n$ converges to zero. For that purpose and analogously to Subsection 3.2, the gradient of the function to be minimized is computed.

Starting from the derivatives

$$\partial_{\Delta\mathbf{m}}\boldsymbol{\epsilon}^{\mathrm{p}}_{n+1} = \mathbb{P}_{\mathrm{dev}} \tag{76}$$

$$\partial_{\Delta\boldsymbol{\epsilon}^{\mathrm{p}}}\boldsymbol{\alpha}_{\mathrm{k}\,n+1} = \frac{-\mathbb{I} - \sqrt{\frac{2}{3}}\,B_{\mathrm{k}}\,\boldsymbol{\alpha}_{\mathrm{k}\,n+1} \otimes \frac{\Delta\boldsymbol{\epsilon}^{\mathrm{p}}}{||\Delta\boldsymbol{\epsilon}^{\mathrm{p}}||}}{1 + \sqrt{\frac{2}{3}}\,B_{\mathrm{k}}\,||\Delta\boldsymbol{\epsilon}^{\mathrm{p}}||} \tag{77}$$

$$\partial_{\Delta\boldsymbol{\epsilon}^{\mathrm{p}}}\alpha_{\mathrm{i}\,n+1} = \frac{-\sqrt{\frac{2}{3}}\,(1 + \alpha_{\mathrm{i}\,n+1}B_{\mathrm{i}})\,\frac{\Delta\boldsymbol{\epsilon}^{\mathrm{p}}}{||\Delta\boldsymbol{\epsilon}^{\mathrm{p}}||}}{1 + \sqrt{\frac{2}{3}}\,B_{\mathrm{i}}\,||\Delta\boldsymbol{\epsilon}^{\mathrm{p}}||}\ , \tag{78}$$

which can be re-written as

$$\partial_{\Delta\boldsymbol{\epsilon}^{\mathrm{p}}}\boldsymbol{\alpha}_{\mathrm{k}\,n+1} = -\mathbb{I} - \sqrt{\frac{2}{3}}\left[B_{\mathrm{k}}\,\boldsymbol{\alpha}_{\mathrm{k}\,n+1} \otimes \frac{\Delta\boldsymbol{\epsilon}^{\mathrm{p}}}{||\Delta\boldsymbol{\epsilon}^{\mathrm{p}}||} + B_{\mathrm{k}}\,||\Delta\boldsymbol{\epsilon}^{\mathrm{p}}||\,\partial_{\Delta\boldsymbol{\epsilon}^{\mathrm{p}}}\boldsymbol{\alpha}_{\mathrm{k}\,n+1}\right] \tag{79}$$

$$\partial_{\Delta\boldsymbol{\epsilon}^{\mathrm{p}}}\alpha_{\mathrm{i}\,n+1} = -\sqrt{\frac{2}{3}}\left[(1 + \alpha_{\mathrm{i}\,n+1}\,B_{\mathrm{i}})\,\frac{\Delta\boldsymbol{\epsilon}^{\mathrm{p}}}{||\Delta\boldsymbol{\epsilon}^{\mathrm{p}}||} + B_{\mathrm{i}}\,||\Delta\boldsymbol{\epsilon}^{\mathrm{p}}||\,\partial_{\Delta\boldsymbol{\epsilon}^{\mathrm{p}}}\alpha_{\mathrm{i}\,n+1}\right]\ , \tag{80}$$

the gradient of the integrated stress power can be computed. After a straightforward computations it results in

$$\begin{aligned}\partial_{\Delta\mathbf{m}} I_{\mathrm{inc}} &= -\mathrm{dev}(\tilde{\boldsymbol{\sigma}}_{n+1}) + \tilde{\mathbf{Q}}_{\mathrm{k}\,n+1} + \sqrt{\frac{2}{3}}\,(\tilde{Q}_{\mathrm{i}\,n+1} + Q_0^{\mathrm{eq}})\,\frac{\Delta\boldsymbol{\epsilon}^{\mathrm{p}}}{||\Delta\boldsymbol{\epsilon}^{\mathrm{p}}||} \\ &\quad + \sqrt{\frac{2}{3}}\,||\Delta\boldsymbol{\epsilon}^{\mathrm{p}}||\,(B_{\mathrm{k}}\,H_{\mathrm{k}}\,\boldsymbol{\alpha}_{\mathrm{k}\,n+1} : \partial_{\Delta\mathbf{m}}\boldsymbol{\alpha}_{\mathrm{k}\,n+1} + B_{\mathrm{i}}\,H_{\mathrm{i}}\,\alpha_{\mathrm{i}\,n+1}\,\partial_{\Delta\mathbf{m}}\alpha_{\mathrm{i}\,n+1})\ .\end{aligned} \tag{81}$$

Accordingly, the gradient converges to

$$\partial_{\Delta\mathbf{m}} I_{\mathrm{inc}} = -\mathrm{dev}(\tilde{\boldsymbol{\sigma}}_{n+1}) + \tilde{\mathbf{Q}}_{\mathrm{k}\,n+1} + \sqrt{\frac{2}{3}}\,(\tilde{Q}_{\mathrm{i}\,n+1} + Q_0^{\mathrm{eq}})\,\frac{\dot{\boldsymbol{\epsilon}}^{\mathrm{p}}}{||\dot{\boldsymbol{\epsilon}}^{\mathrm{p}}||} \quad (\Delta t \to 0). \tag{82}$$

Except for the prefactor $(1-D)$ in Eq. (53), the discrete problem (82) is formally identical to that of the time-continuous case. More explicitly, Eq. (82) implies the flow rule

$$\dot{\boldsymbol{\epsilon}}^{\mathrm{p}} = \sqrt{\frac{3}{2}}\,||\dot{\boldsymbol{\epsilon}}^{\mathrm{p}}||\,\frac{\mathrm{dev}(\tilde{\boldsymbol{\sigma}}) - \tilde{\boldsymbol{Q}}_{\mathrm{k}}}{Q_0^{\mathrm{eq}} + \tilde{Q}_{\mathrm{i}}} \qquad (\Delta t \to 0)\ , \tag{83}$$

as well as the yield function

$$\frac{\partial I_{\text{inc}}}{\partial \Delta \mathbf{m}} : \Delta \boldsymbol{\epsilon}^{\text{p}} \Big|_{\Delta t \to 0} = -\sqrt{\frac{2}{3}}\, ||\dot{\boldsymbol{\epsilon}}^{\text{p}}||\ \phi^{\text{p}} \geq 0 \quad \Leftrightarrow \quad \phi^{\text{p}} \leq 0\ . \tag{84}$$

Thus, the variational principle is indeed consistent. The update is completed by defining the stresses. Again, they follow from

$$\boldsymbol{\sigma}_{n+1} = \partial_{\boldsymbol{\epsilon}_{\boldsymbol{n+1}}} \inf_{\Delta \mathbf{m}} \int_{t_n}^{t_{n+1}} \mathcal{P}\, \mathrm{d}t\ . \tag{85}$$

4.3 The brittle damage model

4.3.1 Fundamentals

By applying a backward Euler time integration scheme to the dissipation (56) as well as to the rate of the Helmholtz energy, the integrated stress power can be written as

$$\begin{aligned} I_{\text{inc}} \;=\; & (1-D_{n+1})\, Y_{n+1} - (1-D_n)\, Y_n \\ & + H_\Gamma\, \frac{\alpha_\Gamma^2}{2}\Big|_{t_n}^{t_{n+1}} + H_{\text{b}}\, \frac{\alpha_{\text{b}}^2}{2}\Big|_{t_n}^{t_{n+1}} + \Delta\lambda^{\text{b}}\, Q_{\text{b}0} \\ & + \Delta\lambda^{\text{b}}\, (N-1)\, Y_{n+1}^N\, \frac{\operatorname{sign}(Y^N-\Gamma)}{S_2} \\ & + \Delta\lambda^{\text{b}}\, (B_\Gamma\, H_\Gamma\, \alpha_{\Gamma\, n+1}^2 + B_{\text{b}}\, H_{\text{b}}\, \alpha_{\text{b}\, n+1}^2)\ . \end{aligned} \tag{86}$$

If the same time integration is also employed for the evolution equations, the updated internal variables (see Eqs. (21)–(23)) can be computed from

$$\alpha_{\Gamma\, n+1} = \frac{\alpha_{\Gamma\, n} - \Delta\lambda^{\text{b}}\, \frac{\operatorname{sign}(Y^N-\Gamma)}{S_2}}{1 + B_\Gamma\, \Delta\lambda^{\text{b}}}\ , \quad \alpha_{\text{b}\, n+1} = \frac{\alpha_{\text{b}\, n} - \Delta\lambda^{\text{b}}}{1 + B_{\text{b}}\, \Delta\lambda^{\text{b}}} \tag{87}$$

and

$$D_{n+1} = D_n + \Delta\lambda^{\text{b}}\, \frac{\operatorname{sign}(Y^N-\Gamma)}{S_2}\, N\, Y_{n+1}^{N-1}\ . \tag{88}$$

With such approximations, the variational constitutive update describing the quasi-brittle damage model reads

$$\Delta\lambda^{\text{b}} = \arg \inf_{\Delta\lambda^{\text{b}}} I_{\text{inc}}\ . \tag{89}$$

4.3.2 Consistency of the algorithm

Starting with the gradient of the integrated stress power

$$\begin{aligned} \partial_{\Delta\lambda^{\text{b}}} I_{\text{inc}} = & -Y_{n+1}\, \partial_{\Delta\lambda^{\text{b}}} D_{n+1} \\ & + H_\Gamma\, \alpha_{\Gamma\, n+1}\, \partial_{\Delta\lambda^{\text{b}}} \alpha_{\Gamma\, n+1} + H_{\text{b}}\, \alpha_{\text{b}\, n+1}\, \partial_{\Delta\lambda^{\text{b}}} \alpha_{\text{b}\, n+1} + Q_{\text{b}0} \\ & + (N-1)\, Y_{n+1}^N\, \frac{\operatorname{sign}(Y^N-\Gamma)}{S_2} + (B_\Gamma\, H_\Gamma\, \alpha_{\Gamma\, n+1}^2 + B_{\text{b}}\, H_{\text{b}}\, \alpha_{\text{b}\, n+1}^2) \\ & + \Delta\lambda^{\text{b}}\, (2\, B_\Gamma\, H_\Gamma\, \alpha_{\Gamma\, n+1}\, \partial_{\Delta\lambda^{\text{b}}} \alpha_{\Gamma\, n+1} + 2\, B_{\text{b}}\, H_{\text{b}}\, \alpha_{\text{b}\, n+1}\, \partial_{\Delta\lambda^{\text{b}}} \alpha_{\text{b}\, n+1}) \end{aligned} \tag{90}$$

and considering the derivatives

$$\partial_{\Delta\lambda^{\mathrm{b}}}\alpha_{\Gamma\,n+1} = -\frac{\operatorname{sign}(Y^N-\Gamma)}{S_2} - B_\Gamma\,\alpha_{\Gamma\,n+1} - B_\Gamma\,\Delta\lambda^{\mathrm{b}}\,\partial_{\Delta\lambda^{\mathrm{b}}}\alpha_{\Gamma\,n+1} \tag{91}$$

$$\partial_{\Delta\lambda^{\mathrm{b}}}\alpha_{\mathrm{b}\,n+1} = \frac{(-1-B_{\mathrm{b}}\,\alpha_{\mathrm{b}\,n+1})}{(1+B_{\mathrm{b}}\,\Delta\lambda^{\mathrm{b}})} = -1 - B_{\mathrm{b}}\left[\alpha_{\mathrm{b}\,n+1} + \Delta\lambda^{\mathrm{b}}\,\partial_{\Delta\lambda^{\mathrm{b}}}\alpha_{\mathrm{b}\,n+1}\right] \tag{92}$$

$$\partial_{\Delta\lambda^{\mathrm{b}}}D_{n+1} = \frac{\operatorname{sign}(Y^N-\Gamma)}{S_2}\,N\,Y_{n+1}^{N-1}\ , \tag{93}$$

this gradient can be re-written as (see Eq. (18))

$$\begin{aligned}\partial_{\Delta\lambda^{\mathrm{b}}}I_{\mathrm{inc}} = (-\phi^{\mathrm{b}}_{n+1}) + \Delta\lambda^{\mathrm{b}}\,(&B_\Gamma\,H_\Gamma\,\alpha_{\Gamma\,n+1}\,\partial_{\Delta\lambda^{\mathrm{b}}}\alpha_{\Gamma\,n+1}\\ &+B_{\mathrm{b}}\,H_{\mathrm{b}}\,\alpha_{\mathrm{b}\,n+1}\,\partial_{\Delta\lambda^{\mathrm{b}}}\alpha_{\mathrm{b}\,n+1})\ .\end{aligned} \tag{94}$$

Consequently, the variational constitutive update (89) is first-order accurate and converges to the continuous problem, i.e.,

$$\partial_{\Delta\lambda^{\mathrm{b}}}I_{\mathrm{inc}}|_{\Delta t\to 0} = -\phi^{\mathrm{b}}_{n+1} \geq 0 \quad\Leftrightarrow\quad \phi^{\mathrm{b}}_{n+1} \leq 0\ . \tag{95}$$

Finally, the updated stresses are obtained from

$$\boldsymbol{\sigma}_{n+1} = \partial_{\boldsymbol{\epsilon_{n+1}}} \inf_{\Delta\lambda^{\mathrm{b}}} I_{\mathrm{inc}}\ . \tag{96}$$

4.4 The coupled ductile-brittle damage model

4.4.1 Update of the state variables

As already pointed out in Subsection 3.4, the coupled ductile-brittle damage model can be efficiently solved by using a staggered scheme, due to the additive structure of the Helmholtz energy and due to two independent failure/yield functions. Within the first step of such a scheme, the minimization problem

$$\Delta\mathbf{m} = \arg\inf_{\Delta\mathbf{m}} I_{\mathrm{inc}}\Big|_{\Delta\lambda^{\mathrm{b}}=0} \tag{97}$$

is computed and the internal variables are updated by Eqs. (73) and (75), i.e., quasi-brittle damage accumulation is ignored. Since problem (97) is numerically relatively expensive, it is only considered in case of plastic loading. For that purpose, the elastic predictor at the trial state $\Delta\mathbf{m} = \mathbf{0}$ is computed and stability of the energy is checked. According to Eqs. (81) and (84), this is equivalent to checking the yield function. If loading is signaled, Eq. (97) is solved by using a Newton scheme combined with a line-search technique, cf. (31). The first-order and the second-order gradients of I_{inc} with respect to $\Delta\mathbf{m}$ necessary for this algorithm are given in Eq. (81) and in the appendix in Eq. (115). It is important to note that convergence of Newton's method has to be checked in the reduced five-dimensional deviatoric space (as implied by the projection (43)). This comment is closely related to the singularity of the Hessian matrix and will be further discussed in Subsection 4.4.3.

Having computed the state variables for the ductile damage model, focus is now a quasi-brittle material degradation. As explained in Subsection 4.3, the degradation mechanisms can be described by the variational principle

$$\Delta\lambda^{\mathrm{b}} = \arg\inf_{\Delta\lambda^{\mathrm{b}}} I_{\mathrm{inc}}\Big|_{\Delta\mathbf{m}=\mathrm{const}} \tag{98}$$

in which the state variables corresponding to ductile deformation have already been computed and updated by means of Eq. (97). The scalar-valued minimization problem (98) is again solved by using Newton's method and loading is checked by stability of the energy at $\Delta\lambda^{\mathrm{b}} = 0$. The first-order and the second-order derivatives necessary for Newton's method can be found in Eq. (90) and in the appendix in Eq. (117).

Knowing all state variables, the stresses can be computed. Similarly to hyperelasticity, they follow from the potential I_{inc}, i.e.,

$$\boldsymbol{\sigma}_{n+1} = \partial_{\boldsymbol{\epsilon}_{n+1}} \left\{ \inf_{\Delta\lambda^{\mathrm{b}}} \inf_{\Delta\mathbf{m}_{n+1}} I_{\mathrm{inc}} \right\} = (1 - D_{n+1})\, \mathbb{C} : \left(\boldsymbol{\epsilon}_{n+1} - \boldsymbol{\epsilon}^{\mathrm{p}}_{n+1}\right) \ . \tag{99}$$

4.4.2 Algorithmic tangent moduli

If Newton's method is also employed at the global level, like typically done in finite element formulations, the linearization of the stress-update algorithm is necessary. Considering Eq. (99), this linearization can be formally written as

$$\begin{aligned} \mathbb{C}^{\mathrm{epd}} := \frac{\mathrm{d}\boldsymbol{\sigma}_{n+1}}{\mathrm{d}\boldsymbol{\epsilon}_{n+1}} = \quad & (1 - D_{n+1})\, \mathbb{C} \\ - \ & (1 - D_{n+1})\, \mathbb{C} : \mathrm{d}_{\boldsymbol{\epsilon}} \boldsymbol{\epsilon}^{\mathrm{p}}\big|_{n+1} - \gamma^{\mathrm{p}}\, \tilde{\boldsymbol{\sigma}}_{n+1} \otimes \mathrm{d}_{\boldsymbol{\epsilon}} D^{\mathrm{p}}\big|_{n+1} \\ - \ & \gamma^{\mathrm{b}}\, \tilde{\boldsymbol{\sigma}}_{n+1} \otimes \mathrm{d}_{\boldsymbol{\epsilon}} D^{\mathrm{b}}\big|_{n+1} \ . \end{aligned} \tag{100}$$

The sensitivities $\mathrm{d}_{\boldsymbol{\epsilon}} \boldsymbol{\epsilon}^{\mathrm{p}}|_{n+1}$, $\mathrm{d}_{\boldsymbol{\epsilon}} D^{\mathrm{p}}|_{n+1}$ and $\mathrm{d}_{\boldsymbol{\epsilon}} D^{\mathrm{b}}|_{n+1}$ can be obtained from linearizing the constitutive update scheme. For instance, by considering the residuals

$$\boldsymbol{R}_{\Delta\mathbf{m}} := \frac{\partial I_{\mathrm{inc}}}{\partial \Delta\mathbf{m}}, \qquad R_{\Delta\lambda^{\mathrm{b}}} := \frac{\partial I_{\mathrm{inc}}}{\partial \Delta\lambda^{\mathrm{b}}} \tag{101}$$

for a converged state, the sensitivity of the plastic strains (more precisely, that of $\Delta\mathbf{m}$) with respect to the currents strains is given by

$$\mathrm{d}\boldsymbol{R}_{\Delta\mathbf{m}} = \mathbf{0} \quad \Rightarrow \quad \mathrm{d}\Delta\mathbf{m} = -\left[\frac{\partial^2 I_{\mathrm{inc}}}{\partial\Delta\mathbf{m} \otimes \partial\Delta\mathbf{m}}\right]^{-1} \cdot \frac{\partial^2 I_{\mathrm{inc}}}{\partial\Delta\mathbf{m} \otimes \partial\boldsymbol{\epsilon}_{n+1}} : \mathrm{d}\boldsymbol{\epsilon}_{n+1} \ . \tag{102}$$

Based on this equation, the derivative of the damage variable D^{p} can be computed by linearizing Eqs. (75) yielding

$$\mathrm{d}D^{\mathrm{p}}_{n+1} = \sqrt{\frac{2}{3}} \left[\frac{(M-1)\, Y^{M-2}}{S_1}\, ||\Delta\boldsymbol{\epsilon}^{\mathrm{p}}||\, \frac{\partial Y}{\partial \Delta\mathbf{m}} + \sqrt{\frac{2}{3}}\, \frac{Y^{M-1}}{S_1}\, \frac{\Delta\boldsymbol{\epsilon}^{\mathrm{p}}}{||\Delta\boldsymbol{\epsilon}^{\mathrm{p}}||} \right] : \mathrm{d}\Delta\mathbf{m} \ . \tag{103}$$

Similarly, the remaining sensitivity is obtained as

$$\mathrm{d}R_{\Delta\lambda^{\mathrm{b}}} = 0 \quad \Rightarrow \quad \mathrm{d}\Delta\lambda^{\mathrm{b}} = -\left[\frac{\partial^2 I_{\mathrm{inc}}}{\partial\Delta\lambda^{\mathrm{b}} \partial\Delta\lambda^{\mathrm{b}}}\right]^{-1} \cdot \frac{\partial^2 I_{\mathrm{inc}}}{\partial\Delta\lambda^{\mathrm{b}} \partial\boldsymbol{\epsilon}_{n+1}} : \mathrm{d}\boldsymbol{\epsilon}_{n+1} \ . \tag{104}$$

4.4.3 Computation of the inverse Hessian matrix for the ductile damage model

Within the Newton scheme defining the ductile damage model, the inverse of the Hessian matrix

$$\mathbb{H} := \frac{\partial^2 I_{\mathrm{inc}}}{\partial\Delta\mathbf{m} \otimes \partial\Delta\mathbf{m}} \tag{105}$$

is required. Unfortunately, a straightforward computation of this inverse by using the relation $\mathbb{H} : \mathbb{H}^{-1} = \mathbb{I}$ is impossible, since $\mathbb{H}$ is singular. This is closely related to the plastic flow rule which has been discretized by the projection method (43). Clearly, such a parameterization cannot be defined uniquely. For instance, if $\Delta\mathbf{m}^{(1)}$ is a solution of the minimization problem $\inf_{\Delta\mathbf{m}} I_{\text{inc}}$, any tensor of the type $\Delta\mathbf{m}^{(2)} = \Delta\mathbf{m}^{(1)} + c\,\mathbf{1}$ $(\forall c \in \mathbb{R})$ is a solution as well. Due to this non-uniqueness, a singular Hessian matrix is expected. As evident, this singularity can be eliminated in a straightforward manner by using the five-dimensional direct parameterization (42). However, the resulting scheme has still shown singularities – particularly, close to a converged state. For this reason, a physically sound and numerically stable pseudoinverse is defined. For deriving this inverse, the classical implicit definition of the inverse via $\mathbb{H} : \mathbb{H}^{-1} = \mathbb{I}$ is projected onto the space of traceless tensors yielding

$$\mathbb{E} : \mathbb{E}^{-1} = \mathbb{P}_{\text{dev}} \ . \tag{106}$$

Obviously, the inverse $\mathbb{E}^{-1}$ depends on the structure of $\mathbb{E}$. According to Eq. (115), it is of the type

$$\mathbb{E} = a_0\,\mathbb{P}_{\text{dev}} + b_0\,\mathbf{m}\otimes\mathbf{m} + c_0\,(\boldsymbol{\alpha}\otimes\mathbf{m} + \mathbf{m}\otimes\boldsymbol{\alpha}) \ . \tag{107}$$

It is expected that the inverse has a similar structure. For this reason, the assumption

$$\mathbb{E}^{-1} = a_1\,\mathbb{P}_{\text{dev}} + b_1\,\mathbf{m}\otimes\mathbf{m} + c_1\,(\boldsymbol{\alpha}\otimes\mathbf{m} + \mathbf{m}\otimes\boldsymbol{\alpha}) + d_1\,\boldsymbol{\alpha}\otimes\boldsymbol{\alpha} \tag{108}$$

is made. Inserting Eqs. (107) and (108) into Eq. (106) leads to the system of equations

$$\begin{aligned}
&a_0\,a_1\,\mathbb{P}_{\text{dev}}\\
&+\mathbf{m}\otimes\mathbf{m}\,(a_1\,b_0 + a_0\,b_1 + b_0\,b_1\,(\mathbf{m}:\mathbf{m}) + (b_0\,c_1 + b_1\,c_0)\,(\boldsymbol{\alpha}:\mathbf{m}) + c_0\,c_1\,(\boldsymbol{\alpha}:\boldsymbol{\alpha}))\\
&+\boldsymbol{\alpha}\otimes\mathbf{m}\,(a_1\,c_0 + a_0\,c_1 + b_1\,c_0\,(\mathbf{m}:\mathbf{m}) + c_0\,c_1\,(\boldsymbol{\alpha}:\mathbf{m}))\\
&+\mathbf{m}\otimes\boldsymbol{\alpha}\,(a_1\,c_0 + a_0\,c_1 + b_0\,c_1\,(\mathbf{m}:\mathbf{m}) + (b_0\,d_1 + c_0\,c_1)\,(\boldsymbol{\alpha}:\mathbf{m}) + c_0\,d_1\,(\boldsymbol{\alpha}:\boldsymbol{\alpha}))\\
&+\boldsymbol{\alpha}\otimes\boldsymbol{\alpha}\,(a_0\,d_1 + c_0\,c_1\,(\mathbf{m}:\mathbf{m}) + c_0\,d_1\,(\boldsymbol{\alpha}:\mathbf{m})) = \mathbb{P}_{\text{dev}} \ .
\end{aligned} \tag{109}$$

As a result, these are five conditions for four unknowns. However, analogously to $\mathbb{H}$ and its inverse, Eq. (109) should be super-symmetric. This condition leads to

$$b_1\,c_0\,(\mathbf{m}:\mathbf{m}) = b_0\,c_1\,(\mathbf{m}:\mathbf{m}) + b_0\,d_1\,(\boldsymbol{\alpha}:\mathbf{m}) + c_0\,d_1\,(\boldsymbol{\alpha}:\boldsymbol{\alpha}) \ . \tag{110}$$

By inserting Eq. (110) into Eq. (109), only four terms remain. Applying ordinary algebraic transformations, the four unknown coefficients can be found as

$$b_1 = \frac{(-b_0^2\,a_0\,(\mathbf{m}:\mathbf{m}) + b_0\,c_0^2\,(\mathbf{m}:\mathbf{m})\,(\boldsymbol{\alpha}:\boldsymbol{\alpha}))}{C} \ , \tag{111}$$

$$c_1 = \frac{-b_0\,(c_0\,a_0\,(\mathbf{m}:\mathbf{m}) + c_0^2\,(\mathbf{m}:\mathbf{m})\,(\boldsymbol{\alpha}:\mathbf{m}))}{C} \ , \tag{112}$$

$$d_1 = \frac{b_0\,c_0^2\,(\mathbf{m}:\mathbf{m})^2}{C} \ , \qquad a_1 = \frac{1}{a_0} \ , \tag{113}$$

with the abbreviation C defined by

$$\begin{aligned}
C = a_0\Big(&2\,c_0\,a_0\,b_0\,(\mathbf{m}:\mathbf{m})\,(\boldsymbol{\alpha}:\mathbf{m}) + c_0^2\,b_0\,(\boldsymbol{\alpha}:\mathbf{m})^2\,(\mathbf{m}:\mathbf{m})\\
&-c_0^2\,b_0\,(\mathbf{m}:\mathbf{m})^2\,(\boldsymbol{\alpha}:\boldsymbol{\alpha}) + a_0^2\,b_0\,(\mathbf{m}:\mathbf{m}) + b_0^2\,a_0\,(\mathbf{m}:\mathbf{m})^2\Big).
\end{aligned} \tag{114}$$

5 Numerical examples

5.1 Low-cycle fatigue behavior of a smooth round bar of Al2024-T351

The accuracy as well as the performance of the novel variational constitutive update are demonstrated here by numerically analyzing the low-cycle fatigue behavior of a smooth round bar of Al2024-T351, cf. (1; 32; 33). The setup of the test and the finite element discretization are schematically shown in Fig. 1. The experimentally observed number of

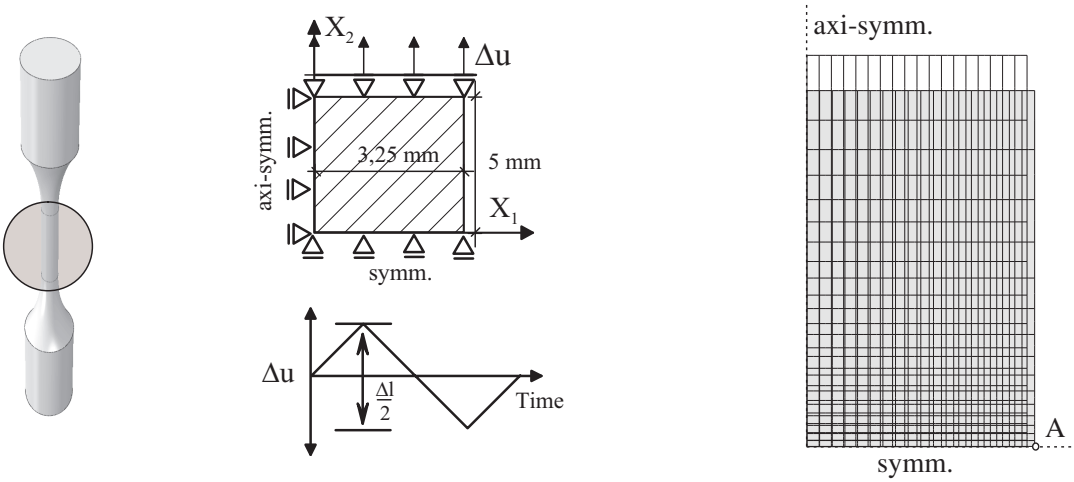

Figure 1: (a) Picture of the smooth round bar; (b) loading conditions; (c) finite element discretization of the undeformed configuration (gray colored) and finite element discretization of the deformed configuration for tension (transparent).

cycles depending on the externally applied strain amplitude $\Delta\epsilon$ can be found in (1).

The aforementioned experiments have been re-analyzed numerically by employing the novel variational constitutive update. Following (1) and in contrast to Subsection 2.1, a superposition of three different kinematic hardening tensors is employed, cf. (34). By doing so, the fitting of the plastic hysteresis can be improved. The material parameters used within the simulations have been taken from (1).

For analyzing the performance of the novel variational constitutive update, its accuracy and the required computing time are compared to those of the classical return-mapping scheme. Both algorithms are based on the staggered solution technique described in Subsection 3.4. Furthermore, the convergence radii have been enlarged by applying a line-search technique, cf. (31).

The predicted lifetimes depending on the prescribed strain amplitudes $\Delta\epsilon$ can be found in Tab. 1. Accordingly, both algorithms lead to similar results. This can be particularly seen in case of a time discretization consisting of 200 steps per loading cycle. Since both methods are based on first-order accurate approximations, this was expected.

Next, the efficiency is analyzed. For that purpose, the computing times are summarized in Tab. 2. It can be seen that the variational update outperforms the classical return-mapping scheme. A more careful analysis reveals that this superiority ($t_{\mathrm{Var}}/t_{\mathrm{Ref}}$) is even more pronounced in case of high strain amplitudes. This is caused by different loading conditions at different prescribed strain amplitudes. More precisely, the number of plastic loading steps is greater the higher the applied strain amplitude. However, since the numerical algorithm for the ductile model is tensor-valued, the number of plastic steps

$\Delta\epsilon$	40 load steps/cycle		100 load steps/cycle		200 load steps/cycle	
	Reference	Variational	Reference	Variational	Reference	Variational
0.04	12.2	12.2	12.2	12.1	12.1	12.1
0.03	35.1	35.7	33.7	34.7	34.7	34.7
0.025	60.0	60.0	59.0	59.0	59.0	59.0
0.02	115.1	115.1	113.0	113.1	113.0	112.2
0.018	163.7	164.2	161.0	161.2	160.1	160.1

Table 1: Numerically predicted number of cycles up to rupture by means of the classical return-mapping algorithm (Reference) and the novel variational constitutive update (Variational).

$\Delta\epsilon$	t_{Ref}	t_{Var}	$t_{\text{Var}}/t_{\text{Ref}}$	$\Delta t = t_{\text{Ref}} - t_{\text{Var}}$	N^{p}	$\Delta t/N^{\text{p}}$
0.04	749.95	580.38	0.773	169.6	720	0.236
0.03	2091.1	1718.9	0.822	372.2	1740	0.214
0.025	3551.8	2924.0	0.823	627.8	2710	0.232
0.02	6875.5	6402.4	0.931	473.1	3620	0.131
0.018	10568.0	9876.9	0.934	691.1	4350	0.159

Table 2: Computing times (in seconds) required for the return-mapping scheme (t_{Ref}) as well as for the variational constitutive update (t_{Var}). The simulations have been performed by using 100 time steps per loading cycle, see Tab. 1. N^{p} is the total number of elastoplastic loading steps up to fracture.

is more decisive for the total computing time. Consequently, dividing the total CPU time by the number of elastoplastic loading steps N^{p} gives an indicator for the efficiency of the algorithm per time step. According to Tab. 2 the related values denoted as $\Delta t/N^{\text{p}}$ vary less significantly than the performance criterion $t_{\text{Var}}/t_{\text{Ref}}$. As a result, it can be concluded that the speedup of the proposed variational constitutive update is mostly due the efficiency of the algorithm for the ductile damage model.

5.2 Stringer-skin connection of a fuselage

In this section, the applicability of the proposed variational constitutive update is demonstrated by a more complex engineering structure. It is a stringer-skin connection of a fuselage. A sketch of the mechanical system, together with the boundary conditions, is shown in Fig. 2 (see also (35)). Although the stringer is bonded to the skin, the whole assembly is considered as homogeneous and no special contact conditions have been defined within the respective finite element simulations. For modeling a pre-existing crack as considered within the respective experiments, an elliptical through-thickness notch is taken, see Fig. 2. The assumption of such a blunt notch reducing stress singularities is very practical from a modeling point of view. Otherwise damage would already evolve from the beginning. As shown in Fig. 2, the structure is loaded by prescribing the displacements at the boundary. In this connection, a symmetric loading amplitude is considered. Within the computations, one loading cycle is discretized by 20 time steps. The set of material parameters used in the numerical analyses is the same as that in (35). For the sake of completeness, it is given in Tab. 3. Further details are omitted here. They can be found

Table 3: Stringer-skin connection of a fuselage: calibrated material parameters for Al 2024-T351 sheets, cf. (35)

Elasticity	
E [MPa]	ν [-]
71000	0.3

Plasticity				
Q_0^{eq} [MPa]	H_i[MPa]	B_i [-]	H_k [MPa]	B_k [-]
345	501.252	5.01252	3333.33	90.0

Stored plastic energy		
m [-]	A [-]	w_{D} [MJ/m^3]
4.964	9.7e-03	1.62

Damage evolution					
M [-]	S_1 [-]	H_Γ [-]	B_Γ [MPa]	γ^{b} [-]	D_{crit} [-]
1.051	2.12	0.052	200.5	0.45	0.23
0.948	2.07	0.112	43.39	0.45	0.23

in (35).

The results of the finite element simulation based on the novel variational constitutive update are shown in Fig. 2. Since the return-mapping scheme leads to almost the same mechanical response, an additional figure is omitted here. The variational constitutive update as well as the return-mapping scheme predict microcrack initiation in the assembly after 60 load cycles. Subsequently, damage evolves fast to the critical value. Analogously to Subsection 5.1, the novel implementation is again computationally more efficient than the conventional return-mapping algorithm. However, due to the relatively large number of degrees of freedom defining the whole finite element mesh, the computation time necessary for solving the respective nonlinear set of equations is significantly higher than the time necessary for the stress update algorithms. For this reason, the overall time (wall clock time) is only marginally smaller for the novel implementation (2%). However, it bears emphasis that the numerical efficiency is only one advantage of the proposed algorithmic formulation. An additional positive feature is the global convergence resulting in an excellent numerical robustness. This is particularly important for highly nonlinear mechanical problems.

6 Conclusions

A variational constitutive update suitable for the analysis of low cycle fatigue in metals has been presented. Within the resulting update, all state variables follow naturally and conveniently from minimizing the stress power of the respective solid. While such variational methods have already been proposed earlier for relatively simple constitutive descriptions, the considered material model is characterized by a complex interplay between plastic deformation, non-linear kinematic hardening, damage accumulation due to void growth as well as quasi-brittle material degradation. For reducing the complexity of the model, a two-step staggered scheme has been used. Within the first step, the ductile damage model was considered. By enforcing the flow rule through a projection technique, the non-associative evolution equations have been derived from an extended variational principle. Mathematically speaking, this can be interpreted as a constrained minimization problem in which the respective constraints have already been explicitly inserted. By discretizing the resulting variational principle, an effective numerical formulation was developed. This formulation is based on a Newton iteration and shows an

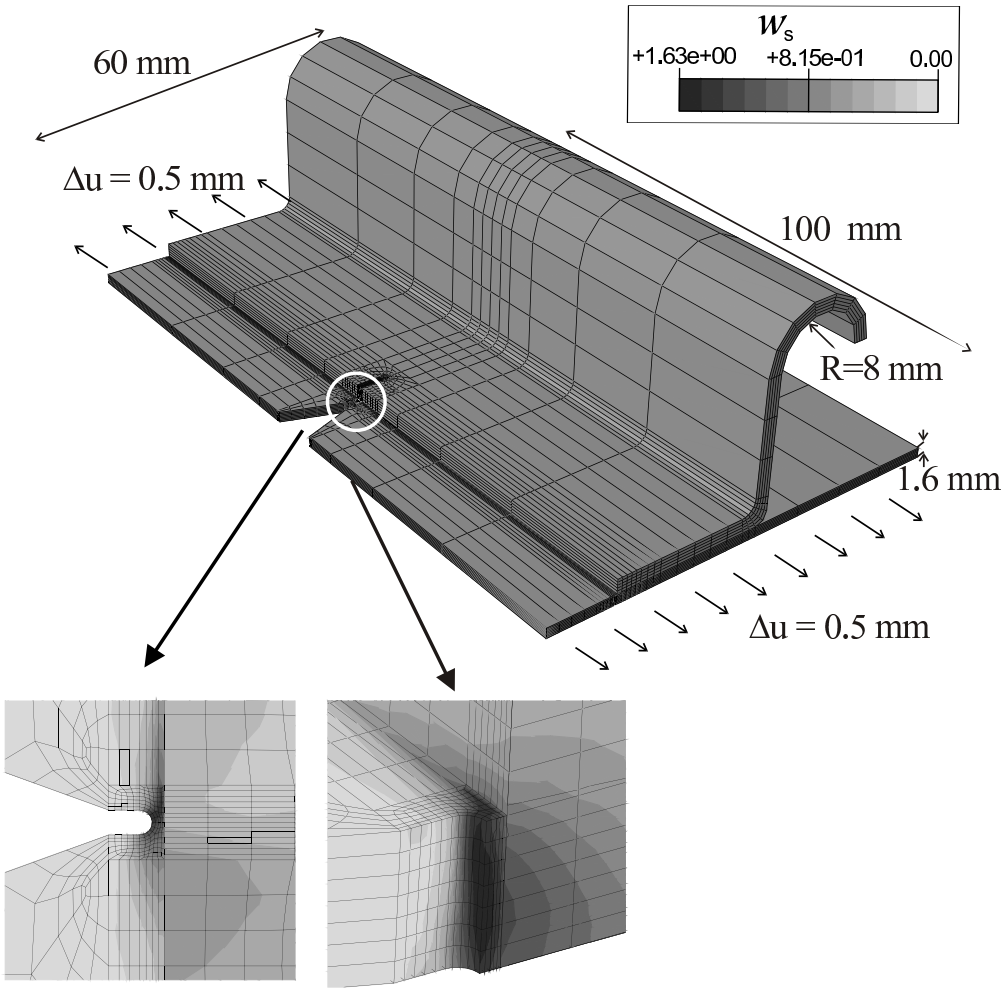

Figure 2: Stringer-skin connection of a fuselage: distribution of the stored plastic energy w_s. Zoom in on the lower left hand side: crack front at the elliptical notch (top view); zoom in on the lower right hand side: profile of plastic stored energy (side view)

asymptotically quadratic convergence. For further increasing the numerical performance of that scheme, a closed-form solution for the inverse of the Hessian matrix has been derived. Since this matrix can become singular, a physically sound pseudoinverse has been defined. The second step of the aforementioned staggered scheme was associated with quasi-brittle damage accumulation. In contrast to previous works on variational updates, the dissipation functional characterizing this material model is not positively homogeneous of degree one. However, a minimization principle could be derived in this case as well. Numerical analyses of low cycle fatigue in a high-strength aluminum alloy have shown the performance of the resulting constitutive update. For all loading cases, it is significantly faster than the classical return-mapping scheme – particularly, if the mechanical response is predominantly elastoplastic.

Acknowledgement

The authors gratefully acknowledge the support of S. Khan and Y. Chen regarding the finite element simulation of the stringer-skin connection of the fuselage as presented in Subsection 5.2.

A Second derivative of the incremental energy defining the ductile damage model

The second-order derivative of the incremental energy (72) defining the ductile damage model reads

$$\begin{aligned}
\frac{\partial^2 I_{\text{inc}}}{\partial \Delta\mathbf{m} \otimes \Delta\mathbf{m}} \;=\;& 2\,\mu\,\mathbb{P}_{\text{dev}} + (Q_0^{\text{eq}} + Q_{\text{i}\,n+1})\,\mathbb{A} \\
&+\frac{H_{\text{k}}}{(1+B_{\text{k}}\,\sqrt{\tfrac{2}{3}}||\Delta\boldsymbol{\epsilon}^{\text{p}}||)^2}\,\Big(\mathbb{P}_{\text{dev}}\,(1+2\,\sqrt{\tfrac{2}{3}}||\Delta\boldsymbol{\epsilon}^{\text{p}}||\,B_{\text{k}}) \\
&+(2\,B_{\text{k}}^2\,\frac{2}{3}\,||\Delta\boldsymbol{\epsilon}^{\text{p}}||)\,\Big(\boldsymbol{\alpha}_{\text{k}\,n+1}\otimes\frac{\Delta\boldsymbol{\epsilon}^{\text{p}}}{||\Delta\boldsymbol{\epsilon}^{\text{p}}||}+\frac{\Delta\boldsymbol{\epsilon}^{\text{p}}}{||\Delta\boldsymbol{\epsilon}^{\text{p}}||}\otimes\boldsymbol{\alpha}_{\text{k}\,n+1}\Big) \\
&+\frac{2}{3}\,||\boldsymbol{\alpha}_{\text{k}\,n+1}||^2\,(-B_{\text{k}}^2+2\,\sqrt{\tfrac{2}{3}}||\Delta\boldsymbol{\epsilon}^{\text{p}}||\,B_{\text{k}}^3)\,\frac{\Delta\boldsymbol{\epsilon}^{\text{p}}}{||\Delta\boldsymbol{\epsilon}^{\text{p}}||}\otimes\frac{\Delta\boldsymbol{\epsilon}^{\text{p}}}{||\Delta\boldsymbol{\epsilon}^{\text{p}}||}\Big) \\
&-\frac{\sqrt{\frac{2}{3}}||\Delta\boldsymbol{\epsilon}^{\text{p}}||\,H_{\text{k}}\,B_{\text{k}}^2}{(1+B_{\text{k}}\,\sqrt{\frac{2}{3}}||\Delta\boldsymbol{\epsilon}^{\text{p}}||)}\,||\boldsymbol{\alpha}_{\text{k}\,n+1}||^2\,\mathbb{A} \\
&+\frac{\frac{2}{3}\,H_{\text{i}}\,(1+\alpha_{\text{i}\,n+1}\,B_{\text{i}})}{(1+B_{\text{i}}\,\sqrt{\frac{2}{3}}||\Delta\boldsymbol{\epsilon}^{\text{p}}||)^2}\,\frac{\Delta\boldsymbol{\epsilon}^{\text{p}}}{||\Delta\boldsymbol{\epsilon}^{\text{p}}||}\otimes\frac{\Delta\boldsymbol{\epsilon}^{\text{p}}}{||\Delta\boldsymbol{\epsilon}^{\text{p}}||} \\
&\Big(1-B_{\text{i}}\,\alpha_{\text{i}\,n+1}+2\,B_{\text{i}}\,\sqrt{\tfrac{2}{3}}||\Delta\boldsymbol{\epsilon}^{\text{p}}||\,(1+B_{\text{i}}\,\alpha_{\text{i}\,n+1})\Big) \\
&-\frac{\sqrt{\frac{2}{3}}||\Delta\boldsymbol{\epsilon}^{\text{p}}||\,H_{\text{i}}\,B_{\text{i}}\,(\alpha_{\text{i}\,n+1}+\alpha_{\text{i}\,n+1}^2\,B_{\text{i}})}{(1+B_{\text{i}}\,\sqrt{\frac{2}{3}}||\Delta\boldsymbol{\epsilon}^{\text{p}}||)}\,\mathbb{A}\;, \qquad (115)
\end{aligned}$$

with

$$\mathbb{A} := \partial_{\Delta\mathbf{m}\otimes\Delta\mathbf{m}}\left\{\sqrt{\frac{2}{3}}||\Delta\boldsymbol{\epsilon}^{\text{p}}||\right\} = \sqrt{\frac{2}{3}}\frac{1}{||\Delta\boldsymbol{\epsilon}^{\text{p}}||}\left(\mathbb{P}_{\text{dev}}-\frac{\Delta\boldsymbol{\epsilon}^{\text{p}}}{||\Delta\boldsymbol{\epsilon}^{\text{p}}||}\otimes\frac{\Delta\boldsymbol{\epsilon}^{\text{p}}}{||\Delta\boldsymbol{\epsilon}^{\text{p}}||}\right). \qquad (116)$$

B Second derivative of the incremental energy defining the quasi-brittle damage model

The second-order derivative of the incremental energy (86) defining the quasi-brittle damage model is given by

$$\begin{aligned}\partial_{\Delta\lambda^{\mathrm{b}}}\partial_{\Delta\lambda^{\mathrm{b}}} I_{\mathrm{inc}} =& \frac{H_\Gamma\,(\frac{\operatorname{sign}(Y^N-\Gamma)}{S_2}+\alpha_{\Gamma\,n+1}\,B_\Gamma)}{(1+B_\Gamma\,\Delta\lambda^{\mathrm{b}})^2}\left(\frac{\operatorname{sign}(Y^N-\Gamma)}{S_2}\right.\\ &-\alpha_{\Gamma\,n+1}\,B_\Gamma\\ &\left.+\,2\,\Delta\lambda^{\mathrm{b}}\,B_\Gamma\,\frac{\operatorname{sign}(Y^N-\Gamma)}{S_2}+2\,\Delta\lambda^{\mathrm{b}}\,B_\Gamma^2\,\alpha_{\Gamma\,n+1}\right)\\ &+\frac{H_{\mathrm{b}}\,(1+\alpha_{\mathrm{b}\,n+1}\,B_{\mathrm{b}})}{(1+B_{\mathrm{b}}\,\Delta\lambda^{\mathrm{b}})^2}\;(1-\alpha_{\mathrm{b}\,n+1}\,B_{\mathrm{b}}\\ &+2\,B_{\mathrm{b}}\,\Delta\lambda^{\mathrm{b}}+2\,\alpha_{\mathrm{b}\,n+1}\,B_{\mathrm{b}}^2\,\Delta\lambda^{\mathrm{b}})\;\;.\end{aligned}\tag{117}$$

References

[1] O. Kintzel, S. Khan, J. Mosler, A novel isotropic quasi-brittle damage model applied to LCF analyses of Al2024, International Journal of Fatigue 32 (2010) 1948–1959.

[2] O. Kintzel, J. Mosler, A coupled isotropic elasto-plastic damage model based on incremental minimization principles, Technische Mechanik 30 (2010) 177–184.

[3] J. Lemaitre, A course on damage mechanics, Springer, Berlin, 1992.

[4] P. Paris, M. Gomez, W. Anderson, A Rational Analytic Theory of Fatigue, The Trend in Engineering 13 (1961) 9–14.

[5] J. Simo, T. Hughes, Computational Inelasticity, Springer: New York, 1998.

[6] M. Ortiz, E. Repetto, Nonconvex energy minimization and dislocation structures in ductile single crystals, Journal of the Mechanics and Physics of Solids 47 (1999) 397–462.

[7] M. Ortiz, L. Stainier, The variational formulation of viscoplastic constitutive updates, Computer Methods in applied Mechanics and Engineering 171 (1999) 419–444.

[8] K. Hackl, F. Fischer, On the relation between the principle of maximum dissipation and inelastic evolution given by dissipation potentials, Proceedings of the Royal Society A: Mathematical, Physical and Engineering Science 464 (2008) 117–132.

[9] J. Mosler, Variational consistent modeling of finite strain plasticity theory with nonlinear kinematic hardening, Computer Methods in Applied Mechanics and Engineering 199 (2010) 2753–2764.

[10] C. Miehe, N. Apel, M. Lambrecht, Anisotropic additive plasticity in the logarithmic strain space: modular kinematic formulation and implementation based on incremental minimization principles for standard materials, Computer Methods in Applied Mechanics and Engineering 191 (2002) 5383–5425.

[11] C. Carstensen, K. Hackl, A. Mielke, Non-convex potentials and microstructures in finite-strain plasticity, Proceedings of the Royal Society London A 458 (2002) 299–317.

[12] H. Petryk, Incremental energy minimization in dissipative solids, Comptes Rendus Mecanique 331 (2003) 469–474.

[13] J. Mosler, O. Bruhns, On the implementation of rate-independent standard dissipative solids at finite strain - Variational constitutive updates, Computer Methods in Applied Mechanics and Engineering 199 (2010) 417–429.

[14] A. Griffith, The phenomena of rupture and flow in solids, Phil. Trans. Roy. Soc. London CCXXI-A (1920) 163–198.

[15] G. A. Francfort, J. J. Marigo, Revisiting brittle fracture as an energy minimization problem, Journal of the Mechanics and Physics of Solids 46 (8) (1998) 1319 – 1342.

[16] B. Bourdin, G. A. Francfort, J.-J. Marigo, Numerical experiments in revisited brittle fracture, Journal of the Mechanics and Physics of Solids 48 (4) (2000) 797 – 826.

[17] A. Chambolle, G. Francfort, J.-J. Marigo, When and how do cracks propagate?, Journal of the Mechanics and Physics of Solids 57 (9) (2009) 1614 – 1622.

[18] B. Bourdin, G. A. Francfort, J.-J. Marigo, The variational approach to fracture, Journal of Elasticity 91 (1-3) (2008) 5–148.

[19] G. Dal Maso, R. Toader, A model for the quasi-static growth of brittle fractures: Existence and approximation results, Archive for Rational Mechanics and Analysis 162 (2) (2002) 101–135.

[20] G. Dal Maso, G. Francfort, R. Toader, Quasistatic crack growth in nonlinear elasticity, Archive for Rational Mechanics and Analysis 176 (2) (2005) 165–225.

[21] E. Lorentz, A mixed interface finite element for cohesive zone models, Computer Methods in Applied Mechanics and Engineering 198 (2) (2008) 302 – 317.

[22] J. Mosler, L. Stanković, R. Radulović, Efficient modeling of localized material failure by means of a variationally consistent embedded strong discontinuity approach, International Journal for Numerical Methods in EngineeringIn press.

[23] J. Mosler, I. Scheider, A thermodynamically and variationally consistent class of damage-type cohesive models, Journal of the Mechanics and Physics of Solids In Press, Accepted Manuscript, in press.

[24] E. Lorentz, V. Godard, Gradient damage models: Toward full-scale computations, Computer Methods in Applied Mechanics and Engineering 200 (21-22) (2011) 1927 – 1944.

[25] C. Miehe, Computational micro-to-macro transitions for discretized micro-structures of heterogeneous materials at finite strains based on the minimization of averaged incremental energy, Computer Methods in Applied Mechanics and Engineering 31 (2003) 559–591.

[26] J. Mosler, O. Bruhns, Towards variational constitutive updates for non-associative plasticity models at finite strain: models based on a volumetric-deviatoric split, International Journal of Solids and Structures 46 (2009) 1676–1684.

[27] Q. Nguyen, Stability and Nonlinear Solid Mechanics, Wiley, 2000.

[28] R. Rockafellar, Convex Analysis, Princeton Landmarks in Mathematics and Physics, 1996.

[29] J. Simo, C. Miehe, Associative coupled thermoplasticity at finite strains: Formulation, numerical analysis and implementation, Computer Methods in Applied Mechanics and Engineering 98 (1992) 41–104.

[30] F. Armero, J. Simo, A priori stability estimates and unconditonally stable product formula algorithms for nonlinear coupled thermoplasticity, International Journal of Plasticity 9 (1993) 749–782.

[31] A. Pérez-Foguet, F. Armero, On the formulation of closest-point projection algorithms in elasto-plasticity - Part II: Globally convergent schemes, International Journal for numerical Methods in Engineering 53 (2002) 331–374.

[32] S. Khan, A. Vyshnevskyy, J. Mosler, Low cycle lifetime assessment of Al2024 alloy, International Journal of Fatigue 8 (2010) 1270–1277.

[33] A. Vyshnevskyy, S. Khan, J. Mosler, An investigation on low cycle lifetime of Al2024 alloys, Journal Key Engineering Materials 417-418 (2009) 289–292.

[34] J. Lemaitre, J.-L. Chaboche, Mechanics of Solid Materials, Cambridge University Press, 1994.

[35] S. Khan, O. Kintzel, J. Mosler, Experimental and numerical lifetime assessment of al2024 sheet, International Journal of FatigueSubmitted.